Department of Radio Science and Engineering

Nanoparticle Sintering Methods and Applications for Printed Electronics

Mark Lee Allen

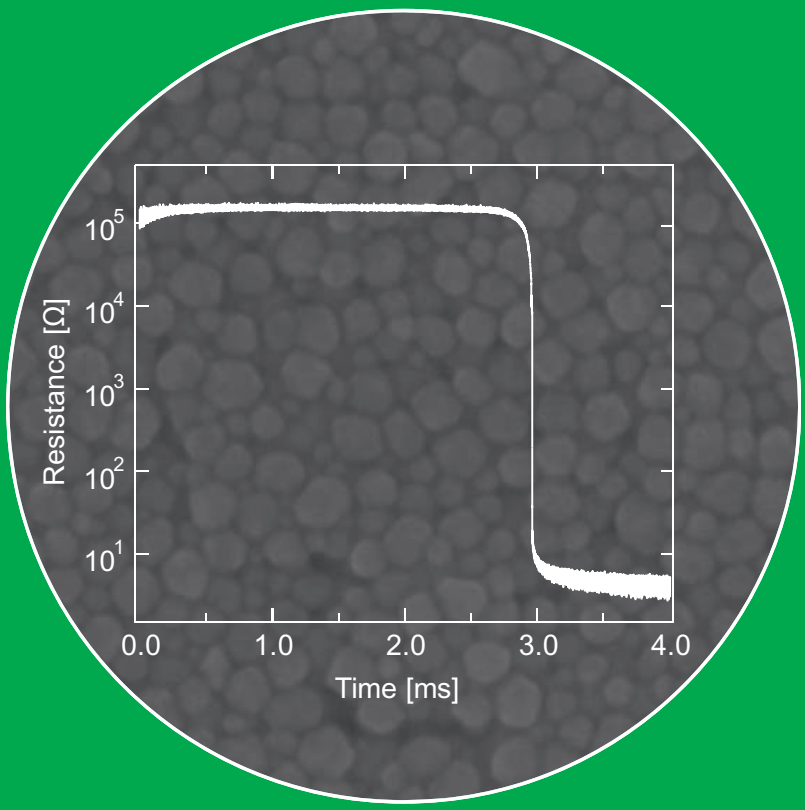

A!

DOCTORAL DISSERTATIONS

Aalto University publication series
DOCTORAL DISSERTATIONS 81/2011

Nanoparticle Sintering Methods and Applications for Printed Electronics

Mark Lee Allen

Doctoral dissertation for the degree of Doctor of Science in Technology to be presented with due permission of the School of Electrical Engineering for public examination and debate in Auditorium S4 at the Aalto University School of Electrical Engineering (Espoo, Finland) on the 19th of October 2011 at 12 noon.

Aalto University
School of Electrical Engineering
Department of Radio Science and Engineering

Supervisor
Prof. D.Sc. (Tech.) Keijo Nikoskinen

Instructor
Prof. D.Sc. (Tech.) Heikki Seppä

Preliminary examiners
Prof. Ph.D. Hans-Erik Nilsson, Mid-Sweden University, Sweden
Ph.D. Matti Mäntysalo, Tampere University of Technology, Finland

Opponent
Prof. Ph.D. Vivek Subramanian, University of California, Berkeley, USA

Aalto University publication series
DOCTORAL DISSERTATIONS 81/2011

ISBN 978-952-60-4278-7 (pdf)
ISBN 978-952-60-4277-0 (printed)
ISSN-L 1799-4934
ISSN 1799-4942 (pdf)
ISSN 1799-4934 (printed)

Aalto Print
Helsinki 2011

Finland

The dissertation can be read at http://lib.tkk.fi/Diss/

Author
Mark Allen

Name of the doctoral dissertation
Nanoparticle Sintering Methods and Applications for Printed Electronics

Publisher School of Electrical Engineering

Unit Department of Radio Science and Engineering

Series Aalto University publication series DOCTORAL DISSERTATIONS 81/2011

Field of research Electromagnetics

Manuscript submitted 17 April 2011 **Manuscript revised** 9 September 2011

Date of the defence 19 October 2011 **Language** English

☐ **Monograph** ☒ **Article dissertation (summary + original articles)**

Abstract

Printed electronics refers to the technologies of fabricating electronic and optoelectronic devices by traditional printing methods. Especially roll-to-roll mass-printing is foreseen to enable low-cost devices on flexible substrates. Direct-write patterning methods, such as inkjet printing, inspire potential for cost-savings in R&D prototyping and customization.

Various organic and inorganic materials can be printed in liquid form and subsequently cured to obtain desired electric functionalities. For example, metals can be printed as nanoparticle dispersions and sintered to obtain high conductivity. In this Thesis, the applicability of silver nanoparticle inks for printed wiring, interconnections, memories, antennas, and wireless resonant tags, is investigated. The Thesis work involves modeling, simulating, fabricating, measuring and analyzing the prototype structures.

Novel methods for sintering nanoparticles are developed. The rapid electrical sintering method, performed by applying voltage over the printed structure, is shown to provide a conductivity increase of more than four orders of magnitude in just milliseconds with the resulting conductivity reaching above 50 % that of bulk silver. The method is further developed to allow for a more practical adaption via contactless coupling at microwave frequencies. A room-temperature sintering method based on the chemical removal of the nanoparticle stabilizing ligand through interaction between the ink and the coating layer of the printing substrate is also presented. The substrate-facilitated sintering method is shown to enable in situ component attachment to printed structures.

Inkjet printed RFID antennas and a wireless RF resonant tag fabricated by a combination of roll-to-roll gravure and inkjet printing are shown to provide reading distances sufficient for many practical applications. A novel approach for contactless read-out of printed memory is introduced and demonstrated for a memory structure inkjet printed using silver nanoparticle ink. The information content of the memory is stored in memory bits selectively programmed using the rapid electrical sintering method.

Keywords Printed electronics, Rapid electrical sintering, Substrate-facilitated sintering, Nanoparticle ink, Inkjet printing, Gravure printing, Radio frequency identification, Printed memory, Interconnection, Contactless read-out

ISBN (printed) 978-952-60-4277-0 **ISBN (pdf)** 978-952-60-4278-7

ISSN-L 1799-4934 **ISSN (printed)** 1799-4934 **ISSN (pdf)** 1799-4942

Location of publisher Espoo **Location of printing** Helsinki **Year** 2011

Pages 93 **The dissertation can be read at** http://lib.tkk.fi/Diss/

Aalto-yliopisto

Tiivistelmä

Aalto-yliopisto, PL 11000, 00076 Aalto www.aalto.fi

Tekijä
Mark Allen

Väitöskirjan nimi
Nanopartikkelisintrausmenetelmät painettavan elektroniikan sovelluksissa ja valmistusprosesseissa

Julkaisija Sähkötekniikan korkeakoulu

Yksikkö Radiotieteen ja -tekniikan laitos

Sarja Aalto University publication series DOCTORAL DISSERTATIONS 81/2011

Tutkimusala Sähkömagnetiikka

Käsikirjoituksen pvm 17.04.2011 **Korjatun käsikirjoituksen pvm** 09.09.2011

Väitöspäivä 19.10.2011 **Kieli** Englanti

☐ **Monografia** ☒ **Yhdistelmäväitöskirja (yhteenveto-osa + erillisartikkelit)**

Tiivistelmä

Painettava elektroniikka käsittää sähköisesti toiminnallisten komponenttien ja rakenteiden valmistamista perinteisiä tulostus- ja painomenetelmiä hyödyntäen. Rullalta rullalle -painomenetelmät mahdollistavat elektroniikan prosessoinnin taipuisalle painoalustalle erittäin halvalla. Digitaaliset suoratulostusmenetelmät, kuten mustesuihkutulostus, soveltuvat erityisesti prototyyppien ja yksilöityjen tuotteiden valmistukseen kustannus-tehokkaasti ja ympäristöystävällisesti.

Lukuisia orgaanisia ja epäorgaanisia materiaaleja voidaan prosessoida nestemuodossa. Esimerkiksi metallisten nanopartikkeleiden matalaa sulamislämpötilaa voidaan hyödyntää johteiden valmistuksessa, kun nanopartikkelimusteena tulostettu kuviointi saadaan sintrattua johteeksi merkittävästi vastaavan metallin sulamislämpötilaa alhaisemmassa lämpötilassa. Tämä väitöskirja käsittelee hopeananopartikkelimusteella painettuja johtimia, komponenttiliitoksia, muistielementtejä, antenneja sekä langattomia resonaattoreita. Väitöskirja sisältää komponenttien mallinnusta, simulointia, valmistusta, mittaamista ja analysointia.

Väitöskirjassa esitellään kaksi uutta sintrausmenetelmää. Väitöstyössä kehitetty sähkösintrausmenetelmä, joka perustuu nanopartikkelikerroksen termosähköiseen takaisinkytkentään, aikaansaa hyvin nopean ja tehokkaan sintrauksen myös lämpöherkillä pinnoilla. Muita menetelmän etuja ovat prosessin energiatehokkuus sekä johtavuuden reaaliaikainen monitorointi ja ohjelmoitavuus. Toinen väitöstyössä kehitetty sintrausmenetelmä perustuu nanopartikkelien pinnoitteen ja painopinnan väliseen kemialliseen reaktioon. Menetelmä mahdollistaa diskreettien komponenttien, kuten mikropiirin, liittämisen suoraan painettuun johdinrakenteeseen ilman erillistä bondausprosessia.

Väitöstyössä osoitetaan hopeananopartikkelimusteella tulostettujen RFID-antennien sekä rullalta rullalle painettujen resonanssipiirien tarjoavan riittävän suorituskyvyn moniin käytännön sovelluksiin. Väitöskirjassa esitellään innovatiivinen kytkentäkonsepti painetun muistin etäluentaan; etälukukonsepti demonstroidaan hopeananopartikkelimusteella tulostetulle muistirakenteelle, jonka informaatiosisältö kirjoitetaan sähkösintraamalla.

Avainsanat Painettava elektroniikka, Sähkösintraus, Substraattiavusteinen sintraus, Nanopartikkelimuste, Mustesuihkutulostus, Syväpaino, RFID, Painettu muisti, Liitostekniikat, Etäluenta

ISBN (painettu) 978-952-60-4277-0 **ISBN (pdf)** 978-952-60-4278-7

ISSN-L 1799-4934 **ISSN (painettu)** 1799-4934 **ISSN (pdf)** 1799-4942

Julkaisupaikka Espoo **Painopaikka** Helsinki **Vuosi** 2011

Sivumäärä 93 **Luettavissa verkossa osoitteessa** http://lib.tkk.fi/Diss/

Preface

The research work of this Thesis was carried out at VTT Technical Research Centre of Finland in Espoo, Finland, and at the joint laboratory between VTT Korea and Konkuk University in Seoul, South Korea, with funding from the Finnish Funding Agency for Technology and Innovation (Tekes), the European Commission, the Technology Industries of Finland Centennial Foundation, the Korea Foundation for International Cooperation of Science and Technology (KICOS), VTT, and Konkuk University. The Thesis was completed at the Department of Radio Science and Engineering of the Aalto University School of Electrical Engineering with funding from the Graduate School in Electronics, Telecommunications and Automation (GETA). Financial support from the Finnish Foundation for Technology Promotion (TES), the Nokia Foundation, the Ulla Tuominen Foundation, and the Finnish Society of Electronics Engineers (EIS) is also gratefully acknowledged.

I wish to express my deepest gratitude to my instructor Prof. Heikki Seppä for sharing his innovative ideas and enthusiasm towards this research topic, and for providing expert advice throughout the work. I also wish to thank Prof. Keijo Nikoskinen for accepting the task of supervising this work and for his continued encouragement to complete this Thesis. I would also like to take this opportunity to thank the pre-examiners, Prof. Hans-Erik Nilsson and Dr. Matti Mäntysalo, for their constructive comments and Prof. Vivek Subramanian for promising to act as the opponent for the public defense of this dissertation.

I am indebted to several current and former colleagues at VTT for their guidance and contribution. I am especially grateful to Dr. Ari Alastalo, Dr. Tomi Mattila, Dr. Mikko Aronniemi, Jaakko Leppäniemi, Kim Eiroma, Mika Suhonen, Kimmo Ojanperä, Dr. Terho Kololuoma, Dr. Marja Vilkman, Kaarle Jaakkola, Dr. Kaj Nummila, Dr. Timo Varpula, Dr. Pekka Pursula, Dr. Panu Helistö, Hannu Sipola, Anssi Rautiainen, Juha-Matti Saari, Ismo Huhtinen, Seppo Kuosmanen, Liisa Hakola, Dr. Tommi Riekkinen, Dr. Arto Hujanen and Matti Somersalo. Furthermore, Dr. Changwoo Lee, Prof. Sunglim Ko, Prof. Keehyun Shin, and colleagues at Konkuk University deserve warm thanks for their hospitality and fruitful collaboration during my working period in Korea.

Finally, I would like to thank my parents for supporting me and most importantly, my wife Tiina and our sons Alex and Nikolas for all their love and patience.

Mark Allen, Espoo, September 2011

Contents

List of Publications

This Thesis is based on the following publications:

I M.L. Allen, M. Aronniemi, T. Mattila, A. Alastalo, K. Ojanperä, M. Suhonen, and H. Seppä, "Electrical sintering of nanoparticle structures," *Nanotechnology*, vol. 19, Apr. 2008, p. 175201.

II A.T. Alastalo, T. Mattila, M.L. Allen, M.J. Aronniemi, J.H. Leppäniemi, K.A. Ojanperä, M.P. Suhonen, and H. Seppä, "Rapid Electrical Sintering of Nanoparticle Structures," *Materials Research Society Symposium Proceedings*, Boston, MA, USA: 2009, p. 1113-F02-07.

III M. Allen, A. Alastalo, M. Suhonen, T. Mattila, J. Leppäniemi, and H. Seppä, "Contactless Electrical Sintering of Silver Nanoparticles on Flexible Substrates," *IEEE Transactions on Microwave Theory and Techniques*, vol. 59, May 2011, pp. 1419-1429.

IV M. Allen, J. Leppäniemi, M. Vilkman, A. Alastalo, and T. Mattila, "Substrate-facilitated nanoparticle sintering and component interconnection procedure," *Nanotechnology*, vol. 21, Nov. 2010, p. 475204.

V M.L. Allen, K. Jaakkola, K. Nummila, and H. Seppä, "Applicability of Metallic Nanoparticle Inks in RFID Applications," *IEEE Transactions on Components and Packaging Technologies*, vol. 32, Jun. 2009, pp. 325-332.

VI M. Allen, M. Aronniemi, T. Mattila, P. Helistö, H. Sipola, A. Rautiainen, J. Leppäniemi, A. Alastalo, R. Korhonen, and H. Seppä, "Contactless read-out of printed memory," *Microelectronic Engineering*, vol. 88, Apr. 2011, pp. 2941-2945.

VII M. Allen, C. Lee, B. Ahn, T. Kololuoma, K. Shin, and S. Ko, "R2R gravure and inkjet printed RF resonant tag," *Microelectronic Engineering*, accepted for publication, 7 p.

These publications are referred to by their Roman numerals [I-VII] throughout the Thesis.

Author's Contribution

I The paper is based on the original electrical sintering invention by the author and Prof. H. Seppä. The author, together with the co-authors, planned the experiments, prepared the samples, carried out the measurements and analyzed the results. The author wrote the first version of the manuscript.

II The author participated in planning, performing and interpreting the results of the experiments, and in finalizing the paper together with the co-authors.

III The author performed all simulations and measurements. He designed the sintering head prototypes and analyzed the results together with the co-authors. The theoretical analysis of power delivery under capacitive biasing conditions is a collaborative effort by Prof. H. Seppä and the author. The author wrote the first version of the manuscript.

IV The substrate-facilitated sintering method presented in the paper was first discovered by the author. The author, together with the co-authors, planned, executed and analyzed the experiments. J. Leppäniemi took the SEM images. The FT-IR spectroscopy measurements and analysis were performed by Dr. M. Vilkman. The author wrote the first version of the manuscript.

V The author planned the experiments, performed the measurements and analyzed the results together with the co-authors. The first version of the manuscript was written by the author and K. Jaakkola.

VI The modulation scheme and memory layout design presented in the paper were first proposed by the author. The author performed the theoretical analysis, simulations and sweep-over measurements. The reader device and software were developed by H. Sipola, A. Rautiainen, Dr. P. Helistö, Dr. R. Korhonen and Prof. H. Seppä. Dr. M. Aronniemi performed the bit-state-switching experiments. The author wrote the first version of the manuscript.

VII The author is responsible for the circuit design, simulations, the inkjet printing work, sample characterization and the electrical measurements. The author participated in the roll-to-roll printing experiments. The author wrote the first version of the manuscript.

Other related publications to which the author has contributed are cited in the text [1-13].

List of Abbreviations and Symbols

AC	Alternating current
AFM	Atomic force microscope
CIGS	Copper indium gallium selenide
DC	Direct current
DSC	Dye-sensitized solar cell
EAS	Electronic article surveillance
EDX	Energy-dispersive X-ray spectroscopy
EIRP	Equivalent isotropically radiated power
FT-IR	Fourier-transform infrared spectroscopy
HF	High frequency
IC	Integrated circuit
ITO	Indium tin oxide
LED	Light emitting diode
OLED	Organic light emitting diode
OTFT	Organic thin-film transistor
PCB	Printed circuit board
PET	Polyethylene terephthalate
PV	Photovoltaic
PVP	Polyvinylpyrrolidone
R2R	Roll-to-roll
RES	Rapid electrical sintering
RF	Radio frequency
RFID	Radio frequency identification
RH	Relative humidity
SEM	Scanning electron microscope
SMA	SubMiniature version A
SUFS	Substrate-facilitated sintering
TCE	Transparent conducting electrode
TEM	Transmission electron microscope
UHF	Ultra high frequency
WLAN	Wireless local area network
WORM	Write-once-read-many
C_1	Coupling capacitance between electrode A and line
C_2	Coupling capacitance between electrode B and line
C_A	Capacitance between electrode A and ground
C_B	Capacitance between electrode B and ground
C_{GND}	Capacitance between line and ground

C_{INT}	Internal capacitance
C_s	Series capacitance
d	Working distance
ε	Emissivity
g	Line spacing
h	Thickness
i	Line index
I	Current
l	Length
n	Number of lines
N	Number of printed layers
P_i	Power dissipated in line i
P_{in}	Input power
P_L	Power dissipated in load
P_{tr}	Power dissipated in nanoparticle structure
$P_{tr,max}$	Peak power dissipated in nanoparticle structure
R_{av}	Average line resistance
R_B	Bit resistance
R_i	Resistance of line i
R_s	Series resistance
R_{Th}	Thévenin equivalent resistance
R_{tr}	Resistance of nanoparticle structure
t	Time
U	Voltage
U_A	Voltage of electrode A
U_B	Voltage of electrode B
U_{DC}	DC voltage
U_{Th}	Thévenin equivalent voltage
v	Velocity
v_N	Normalized read-out voltage
ω	Angular frequency
w	Width
x	Position
Z_L	Load impedance
Z_{Th}	Thévenin equivalent impedance

1. Introduction

1.1 Background

The last decade or so has seen the emergence of a new field of research combining the skills of chemists, physicists, electrical engineers and graphic arts experts to create structures and devices with certain functionalities by means of printing. Instead of serving merely as a graphical pattern, the printed structure now has the purpose of performing some function. A tremendous variety of components can be fabricated by printing to constitute *printed intelligence*. The potential end products include flexible displays, power sources, large-area user interfaces, radio frequency identification (RFID) tags, spoilage indicators on consumer food packages, functional touch-surfaces, disposable diagnostic sensors, etc., operating as stand-alone devices or as part of a larger information system.

The origins of these research activities are often traced back to the discoveries made with the conducting polymer polyacetylene in the late 1970s [14]. Thereafter, a series of technological developments in doping and solution-processing of polymers has created what is referred to today as *organic electronics* (or alternatively *plastic electronics*). The first integrated circuit (IC) based on organic transistors was demonstrated in 1995 [15]. Complementary to polymers, also inorganic materials can be engineered into liquid form to enable solution-processing. For example, metallic and semiconducting nanoparticle inks can provide improvements in material properties such as conductivity, semiconductor charge-carrier mobility, and environmental stability with respect to their organic counterparts [16-20]. Hence, the term *printed electronics* best describes this set of technologies for electronics manufacturing using functional inks and conventional printing methods as well as the diverse multitude of the electronic products assembled this way.

1.2 Motivation

Printed electronics is not being developed to replace silicon-based electronics; the integration density and electric performance obtained by etching the surface of single-crystal silicon wafers at high resolution, and the corresponding cost per function, are far beyond what any combination of inks and printing methods can offer. Nonetheless, the estimated market potential of printed electronics is huge with annual revenues projected at above $50 billion by 2020 [21]. Here, the promise is the advent of large-area devices typical of comprising a low fill-factor pattern and/or several thin material layers, which can be manufactured in high-volumes on very low-cost substrates.

Some of the recently demonstrated printed electronics components include organic light emitting diodes (OLED) [22-24], photovoltaics (PV) [25-27], transistors [20,28-33], passive electric components [34], interconnecting circuit wiring [35,36], antennas [37-39], memories [4,40-42], and sensors [43-47]. The challenge is in that many of the conceivable applications that first spring to mind (e.g. printed visitor access cards, low-cost temperature/time logging electronic tags, or perhaps an interactive screen on a Happy Meal™ box) often impose high requirements on circuit complexity and set strict manufacturing specifications accordingly. Although various applicable circuit components (e.g. high frequency (HF) rectifiers [48] and transistors demonstrating GHz-operation [49]) and fully functional devices (e.g. a 1-bit RFID tag [50]) can be achieved by using state-of-the-art inks and high-resolution printing tools [51,52], it has yet to be proven whether the all-printed electronics approach will ultimately lead to more cost-effective manufacturing than is obtained with hybrid solutions comprising microchips attached to printed circuitry [53]. On the other hand, by relaxing the feature size and tolerance requirements to ascertain yield and cost demands are met, we quickly limit the scope of attainable products with a viable market [54]. That is to say that printed electronics may very well revolutionize our daily lives by enabling ubiquitous tags, screens, touch-panels, sensors or what have you, but these solutions will probably be enabled only by a combination of a printed large-area platform and one or several extremely small silicon microchips interconnected to the printed wiring via some cost-effective chip attachment procedure.

Printed electronics is highly materials-oriented: (i) the inks must perform as stable dispersions with carefully tuned viscosity and surface-tension values for printing while (ii) the transferred material films provide the necessary electronic

functionality in the end product, such as charge transport via interlinked molecules or particles. The challenge is that these requirements often impose contradicting demands on ink composition. This is the case, for example, with metallic nanoparticle inks, where the particles must be capped with a protective shell to obtain a stable dispersion but, on the other hand, a tightly bound capping layer means that rather high temperatures are required to anneal (sinter) the printed structure. The efficiency of sintering, i.e. the degree with which the adjacent nanoparticles are fused together to form a continuous structure, directly reflects conductivity. Particularly for applications requiring as low-resistance wiring as possible (e.g. RFID coil antennas and conductor grids on optoelectronic devices), the resulting conductivity (efficiency of material usage) scales directly with material costs.

Nanoparticle sintering is typically carried out by heating the printed structure in an oven or on a hotplate; near-bulk conductivity can be obtained by curing at above ca. 200 °C for a duration of several minutes [18,55,56]. These conditions are often challenging for low-cost substrates (due to e.g. shrinkage and gas emissions) and limit processing speeds on high-throughput roll-to-roll (R2R) printing lines. Hence, various alternative sintering methods have been recently introduced to overcome some of these limitations. These include at least laser sintering [57-61], pulsed light sintering [62-65], microwave sintering [66,67], chemical sintering [68-70], and plasma sintering [71].

1.3 Scope and Contents of the Thesis

This Thesis contributes to printed electronics by introducing novel room-temperature sintering methods and applications thereof. The rapid electrical sintering (RES) method provides (i) extremely short sintering times (conductivity increase of several orders of magnitude in just milliseconds), (ii) reduced substrate heating to enable processing also on temperature-sensitive surfaces, (iii) energy-efficient processing, (iv) real-time monitoring of the process, and (v) excellent quality (above 50% of bulk silver conductivity thus far demonstrated). The method is further developed to enable contactless processing over a constantly moving substrate emulating a R2R printing environment. RES lends itself readily to memory applications by enabling a low-voltage operated write-once-read-many (WORM) type all-printed memory. In this Thesis, a contactless coupling scheme for read-out of the information content of a printed memory of this kind is also introduced and demonstrated. The second method, substrate-

facilitated sintering (SUFS), is based on the removal of the particle capping layer (stabilizing ligand) through interaction with a chemically matched ink-receptive substrate coating layer. This way, the exposed metallic nanoparticles are released into contact whereafter sintering progresses towards a thermodynamic equilibrium under ambient conditions. Furthermore, SUFS is shown to enable direct interconnection of discrete components to printed wiring. This approach can provide extremely cost-effective component assembly via inline printing and chip placement to realize hybrid solutions. The performance of inkjet printed RFID antennas and gravure printed passive radio frequency (RF) circuitry is also studied.

This Thesis overview begins with an introduction to the materials and methods deployed in the work (Chapters 2 and 3). Thereafter, the scientific results and findings of the publications [I-VII] are summarized in Chapters 4, 5 and 6. The developed technologies and applications are discussed and critically evaluated in Chapter 7. The conclusions are presented in Chapter 8.

2. Printing of Functional Materials

A multitude of functional materials can be engineered into liquid form to produce e.g. electroluminescent, semiconducting, or metallic layers using traditional graphic arts printing methods [16,22,28,29,31,72,73]. The optimal ink composition is often a trade-off between solubility and the final obtained electronic functionality. For complete printed devices, control of ink-substrate and interlayer interactions such as adhesion, wetting and diffusion phenomena has a large impact on performance. In this Chapter, some of the printing methods employed in printed electronics research and manufacturing are described. Ink behavior on the substrate surface and multi-layer printing are also briefly discussed.

2.1 Printing Methods

Electronic inks are printed using either contact-mode template or contactless direct-write methods onto a web-fed (R2R) or sheet-fed substrate. With contact printing techniques such as gravure, flexography or screen printing, the ink is transferred onto the substrate via an image-carrying master template. Direct-write patterning methods enable printing directly from digital format.

In gravure printing, the surface of a metallic printing cylinder is patterned as a raster of small cells, which hold the ink while excess ink is removed by a doctor blade during printing. The amount of ink transferred from the cells onto the printing substrate is dependent on cell shape and volume as well as the ink properties and the operating parameters applied [74]. R2R gravure printing is particularly suitable for high volume printing of thin layers of uniform thickness [73] as demonstrated for OLEDs in [23,24]. Similarly, gravure has been used for printing the semiconducting and dielectric layers of organic thin-film transistors (OTFT) [29,30,33,73]. Conductors can be gravure printed from silver nano-

particle ink [50,75,VII] to provide high-resolution patterning with line widths of 20 μm [30,52] demonstrated at best.

Flexographic printing utilizes a rubber or polymer relief on a cylinder to transfer the image. Compared to gravure, flexographic printing can be performed with minimal pressure between the cylinder and substrate so that printing over sensitive layers is possible [73]. This method is compatible with organic [29,76] and inorganic [38,73] materials alike although the rubber relief does impose some constraints on the variety of chemically compatible solvents.

Screen printing is applied by moving a squeegee across a patterned mesh stencil, which enables ink transfer though the image areas onto the substrate. Screen printing with silver flake pastes has been widely applied for fabricating RFID antennas [12,13,77] and photovoltaic metallizations [78,79] although e.g. screen printed OTFTs have also been reported [80]. The thickness of silver paste screen printed layers can reach ca. 20 μm. Here, the electrical conductivity typically obtained after thermal curing (electrical conductivity arises through reduced contact resistance between micron-size silver flakes in a polymer matrix) is at least a decade lower than can be obtained via silver nanoparticle sintering. Hence, the resulting sheet resistance is roughly equivalent for screen printed thick-film conductors and inkjet printed nanoparticle conductors with thicknesses typically in the micron range. Flexographic plates and screen meshes are cheaper than engraved gravure cylinders, which makes these methods more attractive for testing and manufacturing of small batches.

A R2R printing line may comprise several printing units allowing for each material layer to be printed using the best suited method, respectively. Figure 1(a) shows the R2R printing system employed at the Flexible Display Research Centre of Konkuk University, where the printing work of [VII] was carried out. The numbering (1)-(13) indicates the sequence of units through which the web flows in the system. In Figure 1(b), a dielectric layer is gravure printed over underlying conductor patterning at a web speed of 5 m min^{-1}. Here, the cell depths of the gravure cylinders for the conducting and dielectric layers were etched to 18 μm and 42 μm, respectively [VII].

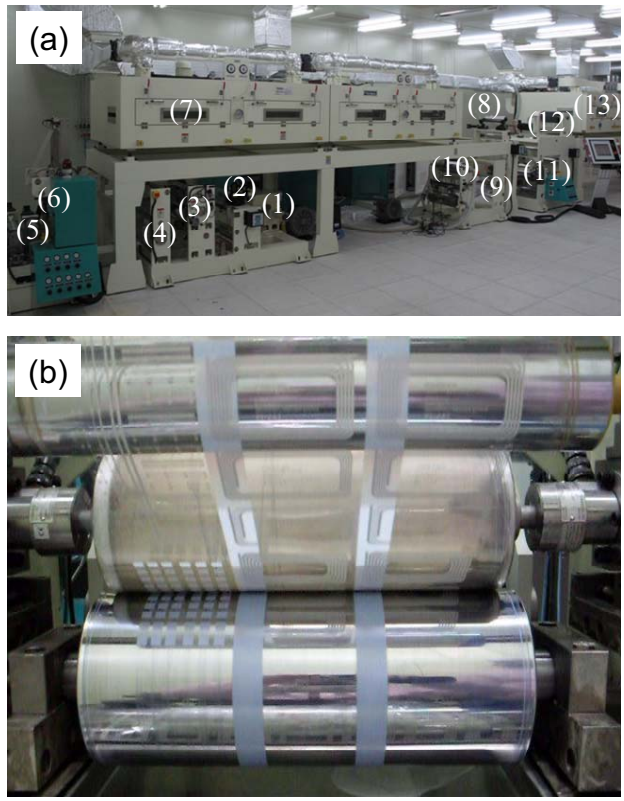

Figure 1. (a) R2R printing system: (1) unwinding unit, (2) edge positioning unit, (3) infeeding unit, (4) preheating unit, (5) flexo-printing unit, (6) direct gravure printing unit, (7) hot air drying unit, (8) edge positioning unit, (9) cooling unit, (10) non-contacting transportation unit, (11) gravure offset printing unit, (12) suction roll, and (13) hot air drying unit. (b) Direct gravure printing of conducting coil patterning and dielectric layer [VII].

Direct-write methods enable contactless deposition of functional materials to generate a printed replica of a digital image. Inkjet printing is by far the most widely applied direct-write patterning method [81,82] although other methods, such as Aerosol Jet printing[1], are also attractive especially for rapid prototyping

[1] Aerosol Jet is a registered trademark of Optomec, Inc. http://www.optomec.com

and for highly customized printed electronics applications [83-85]. A range of vendors offer piezoelectric drop-on-demand inkjet printheads and systems for laboratory-scale materials testing through to industrial-scale manufacturing. Here, a piezoelectric actuator in the printhead expands in response to a voltage pulse causing a pressure wave in the liquid, and expelling a single droplet though the nozzle [82,86]. The in-flight drop diameter is directly related to the diameter of the nozzle and is typically in the range of 10-100 μm [87,88]. However, also submicron patterning resolution has been demonstrated with a custom-built inkjet system [51]. Inkjet has been applied for printing transistors [28,31,32,89], OLEDs [22], photovoltaics [25,26], antennas [37,V], memories [4,41,VI], sensors [43,44,46,47], and many other components and devices.

The inkjet printing work of this Thesis is performed using the single-nozzle Autodrop system (Microdrop Technologies GmbH), the DMP-2831 desktop printer (FUJIFILM Dimatix, Inc.), and the pilot-scale XY-MDS2.0 sheet-fed printer (iTi, Inc.) driving a Spectra SX-128 printhead (FUJIFILM Dimatix, Inc.). A significant benefit related to single-nozzle printing is the possibility to print in vector-graphics mode, where the printhead follows the print pattern also for curvilinear geometries. Figure 2(a) visualizes the drop formation on the Autodrop system as a temporal sequence of images. The fluid first emerges from the nozzle as a drop followed by a ligament tail, which eventually collapses into the droplet so that a spherical drop is formed by the point at which the ink impacts the substrate. The DMP's cartridge-style printheads have 16 nozzles linearly spaced at 254 μm, where the nominal drop volume is either 1 or 10 pL according to the cartridge type. Figure 2(b) shows RFID dipole antenna printing on the DMP; the cartridge is turned at an angle to adjust the printing resolution. The XY-MDS2.0 system with a Spectra SX-128 printhead was used in [IV] and [VI] for jetting silver nanoparticle ink at 100 mm s^{-1} head speed and 600 dpi printing resolution. Also here, the inter-nozzle distance (native resolution) is larger than the inter-drop distance (print resolution) and multiple passes are required to complete the pattern. The scanning electron microscope (SEM) image of Figure 2(c) shows a polyimide dielectric line printed (with the pilot-scale iTi system) over a 60 μm high chip edge demonstrating the capability of inkjet for printing over 3-D topologies [90].

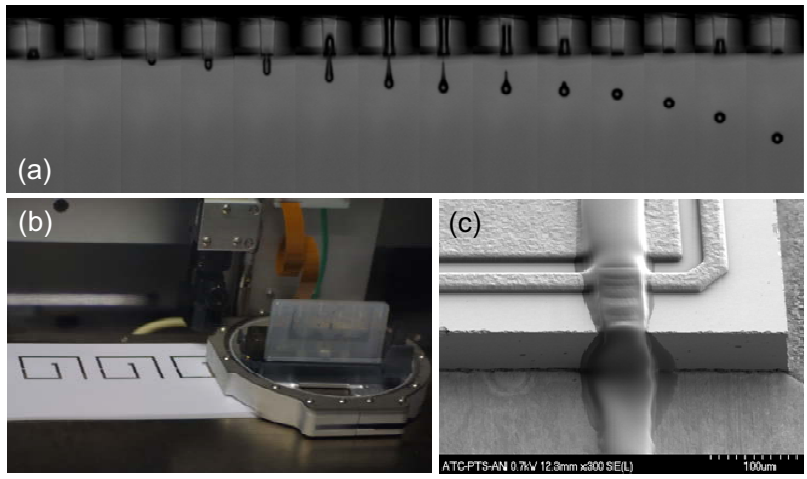

Figure 2. (a) Drop formation on the Autodrop single-nozzle inkjet printer[2]. (b) Antenna printing on the DMP-2831 desktop inkjet printer. (c) SEM image of a dielectric line inkjet printed over a 60 µm chip edge (Reprinted from [90], Copyright (2010), with permission from Elsevier) [3].

2.2 Ink Behaviour on Receptive Surface

A challenge with applying printing methods beyond their commonplace graphics use for fabricating electronic structures is obtaining smooth and continuous material layers. While a pixilated inkjet or gravure printed pattern can appear smooth to the naked eye, any single discontinuity in a conductor or pinhole in an insulating layer is cause enough for device failure. Hence, an appropriate degree of wetting on the receptive surface is desirable to achieve adequate pixel overlap while maintaining a high feature resolution.

[2] Courtesy of K. Ojanperä of VTT

[3] The printing work of [90] was carried out at VTT by K. Eiroma and the author as part of a contract research project.

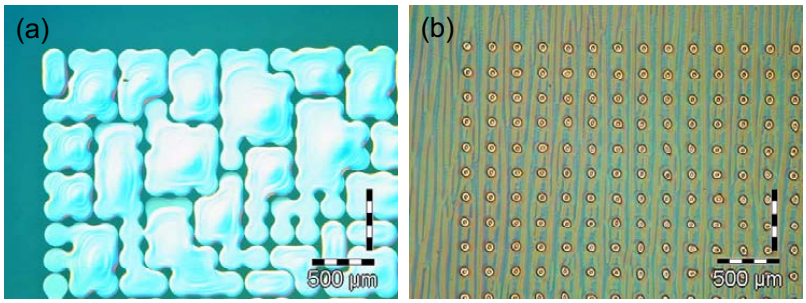

Figure 3. Inkjet printed silver nanoparticle ink on (a) bare glass slide demonstrating strong wetting and (b) surface-treated glass slide proving a small drop diameter. The printing was carried out at 200 µm droplet spacing with a 50 µm printhead nozzle diameter.

The chemical and physical processes governing drop impact on a solid surface and subsequent spreading via inertial, surface tension and capillary forces, as well as the coalescence of neighboring liquid drops, are thoroughly studied in the context of inkjet printing [88,91]. The equilibrium contact angle of the drop with the receptive surface and drop spacing greatly affect the pattern dimensions obtained [91]. This is visualized in Figure 3 with an array of drops inkjet printed at 200 µm spacing onto a bare glass slide in Figure 3(a) and a glass slide dip-coated with a fluoropolymer surface treatment solvent (Novec EGC-1700 supplied by 3M, Inc.) in Figure 3(b). This pre-treatment procedure significantly decreases the surface energy of the glass slide to promote anti-wetting of the silver nanoparticle ink (Silverjet DGP-45LT-15C, supplied by Advanced Nano Products Co. Ltd., was applied here).

The print dimensions can be further controlled by adjusting the temperature of the substrate. For example, high resolution features are obtained by immobilizing and solidifying the drops immediately upon impinging on the hot substrate. This approach, however, is often limited by the thermal budget of the substrate.

When printing on substrates coated with a porous, ink-receptive layer, such as inkjet photopapers, both spreading and infiltration processes coexist and somewhat compete [88]. The coated polyethylene terephthalate (PET) substrate of Figure 4(a) reveals the principle of particle fixation at the drop location while the ink solvent is absorbed into an underlying layer and transported also outside the target areas [IV]. Figure 4(b) shows lines inkjet printed on photopaper as a series of overlapping drops at a relatively large inter-drop spacing.

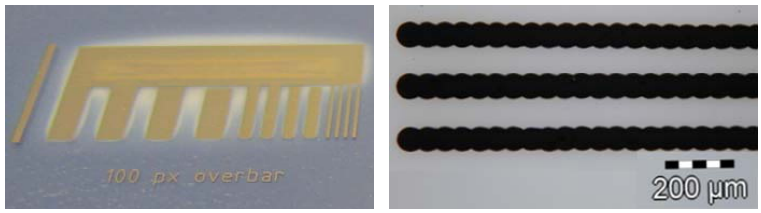

Figure 4. Inkjet printed silver nanoparticle patterning on coated substrates. (a) The coating layer provides particle fixation at the drop location while the solvent is pulled into an underlying layer (visible as a glare around the printed pattern). (b) Line formation by printing a sequence of overlapping drops.

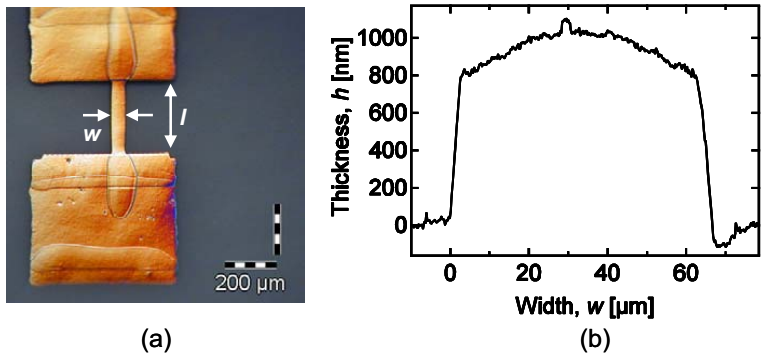

Figure 5. (a) Optical microscope view of inkjet printed narrow line between contact pads. (b) AFM profile scan over the line [I].

Nanoparticle inks designed for inkjet or gravure printing have low solid contents (corresponding to a few volume percent). When printed on a non-absorbing surface, the printed layer thus undergoes a significant reduction in volume upon solidification resulting in a dry layer thickness typically of the order of one micron [V]. Similar layer thicknesses are obtained by printing on coated substrates, in which case the solvent is removed via absorption rather than evaporation. In [I], a silver line equivalent to that imaged in Figure 5(a) was inkjet printed on photopaper to provide a line thickness and width of h = 900 ± 100 nm and w = 60 ± 10 µm, respectively. The corresponding atomic force microscope (AFM) scan across the width of the line is shown in Figure 5(b).

2.3 Multilayer Printing

Most printed electronics components and devices are assembled by printing more than one material layer. Furthermore, printing successive layers is required in some applications to increase the thickness of a certain layer, e.g. the metal wiring of RFID coil antennas [V]. Although layering of materials is one of the strengths associated with printing methods for electronics manufacturing, multilayer printing imposes further material and process-related prerequisites: (i) controlling the fluid dynamics on a previously printed layer, for which the surface chemistry and roughness can significantly deviate from that of an optimized substrate surface, is often challenging, (ii) the printed materials must be cross-compatible in that e.g. the ink solvent or nanoparticles will not dissolve or migrate through the underlying layer, and (iii) each layer must be aligned correctly with respect to the underlying patterning (an optical fiducial camera or punched registration holes are often applied [92,93]). The microscope image of Figure 6 shows gravure printed conducting and insulating layers followed by an inkjet printed conducting layer. Here, the insulating second layer is pinhole-free even though the first layer possesses a high surface roughness [VII].

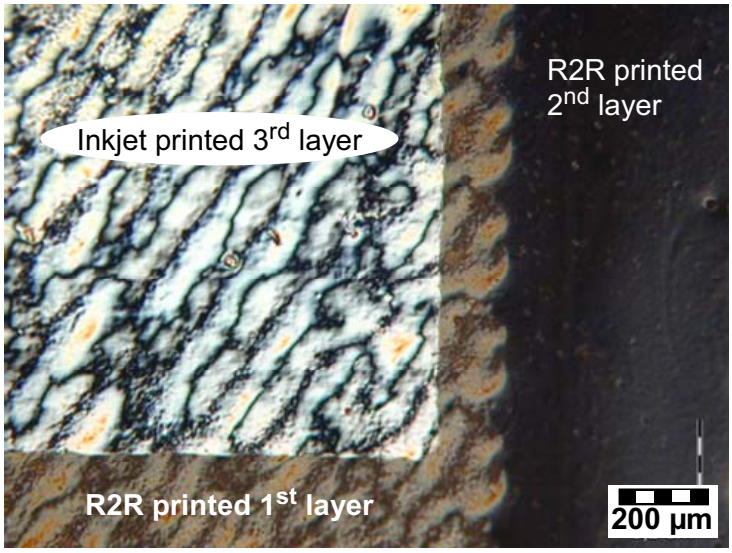

Figure 6. Inkjet and gravure printed multilayer structure [VII].

3. Nanoparticle Inks

Nanoparticle inks are increasingly exploited in printed electronics for realizing conductors [18,19,56], transparent electrodes [94], transistors [16,20], and several other structures. Metallic nanoparticles (silver [18,19,56] is most widely applied although e.g. gold [19,34] and copper [95-97] have also been studied) enable inkjet or R2R printing of high quality conductors on low-cost, flexible substrates. Here, the nanoparticles are usually capped with a protective ligand shell to prevent particle agglomeration when dispersed in the liquid vehicle [98,99]. Once printed, a continuous metallic structure is obtained by evaporating or absorbing the ink solvent and sintering the nanoparticles.

3.1 Size-dependent Melting Temperature

Metallic particles in the size range of 1-100 nm have remarkable electronic and structural properties [100,101] significantly altered from those of either the bulk or the corresponding single atom. It is well-established experimentally that the melting temperature of metallic nanoparticles decreases with decreasing particle size [101-103]. Although various proposed theoretical models have been shown to provide a reasonable fit to the experimental data [101,104-106], understanding the surface interactions and the internal arrangement of atoms is a complex task [107,108]. Nonetheless, the general prediction of these models is that the lowering of the melting temperature is directly proportional to the surface-to-volume ratio of the nanoparticle; the physical interpretation being that the surface atoms are less constraint in thermal motion because of reduced atomic coordination numbers relative to the bulk [107]. This unique property is exploited in low-temperature curable conductive nanoparticle inks such as the kind studied in this Thesis.

3.2 Sintering

The nominal particle diameter in metallic nanoparticle inks typically ranges from 2 to 60 nm [16,18,19,34,56,95,109,I-VII]. A capping ligand is applied to keep the metal particle cores detached and to provide solubility. Thiol ligands [98] provide a high binding strength to the metal core and result in a more stable ink than can be obtained with polymer ligands [99]. Similarly, also the energy required for breaking the particle-ligand bonds to allow for physical contact between the particles after printing, is higher. For this reason, polymer ligands are often utilized in low-curing temperature silver nanoparticle inks. The transmission electron microscope (TEM) image of Figure 7(a), obtained by thinning silver nanoparticle ink (Inkjet Silver Conductor AG-IJ-G-100-S1 of Cabot Printable Electronics and Displays, Inc.) with ethanol and ethylene glycol and placing a drop onto the TEM grid, reveals the polymer layer encapsulating the silver nanoparticle core to have a thickness of ca. 1 nm.

The nanoparticle layer is usually electrically insulating immediately after printing. Thereafter, the solvent is removed to provide a network of closely-packed ligand-separated nanoparticles as shown in Figure 7(b) for silver nanoparticle ink (Inkjet Silver Conductor AG-IJ-G-100-S1 of Cabot Printable Electronics and Displays, Inc.) printed on polyimide. Throughout this Thesis, this is considered as the initial nanoparticle structure prior to sintering.

Sintering takes place as the particle-ligand bonds are broken and the exposed nanoparticle cores are released into contact [68,IV]. Nanoparticle coalescence progresses with the formation of neck structures at the particle interfaces prima rily driven by the surface energy reduction experienced as the particles fuse [110][4]. High conductivity is achieved through these percolation channels interconnecting the adjacent particles rather than through complete collapse into bulk metal [42,111,IV]. Figure 7(c) provides a SEM image of sintered silver nanoparticles on polyimide demonstrating a major structural change from that of the corresponding initial unsintered state in Figure 7(b).

---

[4] Many physical processes are manifested in nanoparticle sintering including interparticle capacitive and Van der Waals forces, chemical reactions, decrease of total surface energy, diffusion, capillary effects, viscous flow, phase transitions, etc. The derivation of an accurate nanosintering model beyond classical “large particle” sintering theories [112] is a subject of ongoing study [158].

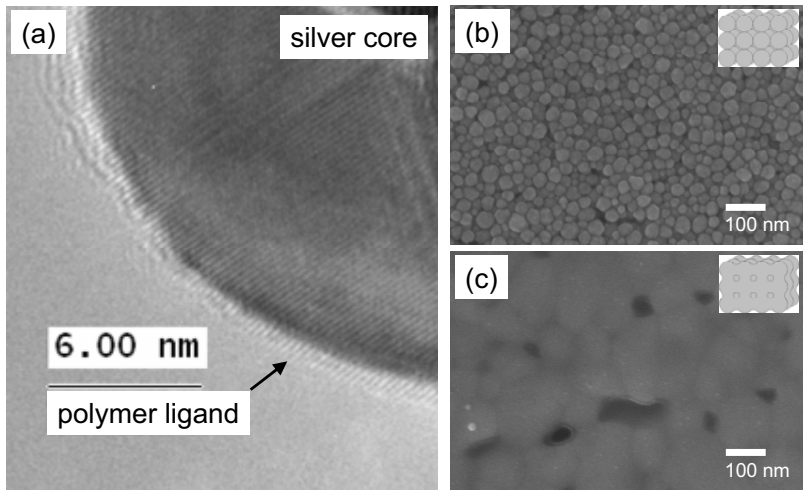

Figure 7. (a) TEM image of part of a silver nanoparticle encapsulated with a polymer shell[5]. SEM images of inkjet printed silver nanoparticles on polyimide (b) before and (c) after sintering[6]. The insets are provided to schematically illustrate the structural change the nanoparticle layer undergoes during sintering.

Nanoparticle sintering is usually accomplished by heating in an oven/furnace or on a hotplate. Depending on the particle size and the binding strength of the ligand shell, the sintering temperatures are typically around 100-400 °C [18,97,111]. The measured sheet resistance of lines of various widths inkjet printed with silver nanoparticle ink on polyimide and oven sintered at 240 °C for 15 min is shown in Figure 8. A linear dependence between sheet resistance and the inverse of the number of printed layers is apparent in Figure 8 from which a corresponding conductivity of 16 MS m^{-1} was computed in [V].

[5] The TEM imaging was carried out by Dr. H. Jiang of Aalto University together with the author.

[6] The SEM imaging was carried out by Dr. M. Aronniemi (currently with Vaisala Oyj) together with the author at VTT.

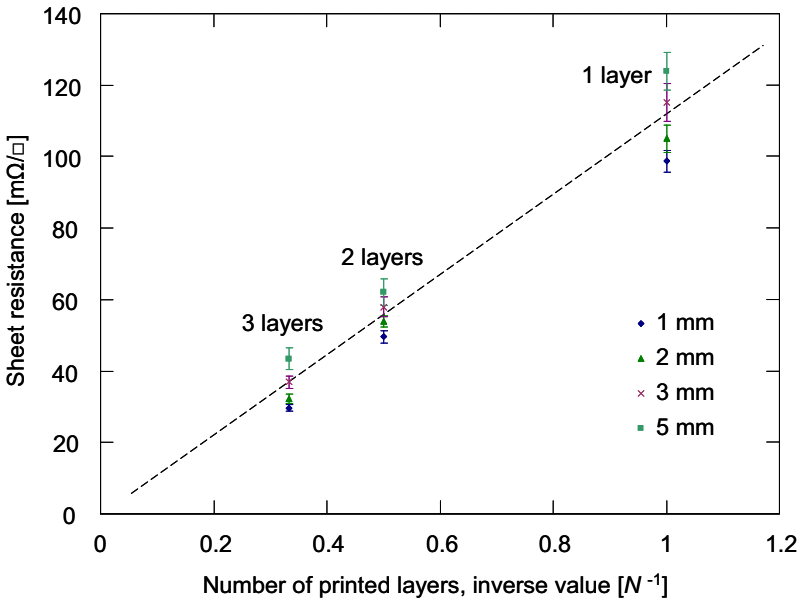

Figure 8. Sheet resistance of silver nanoparticle lines inkjet printed on polyimide and sintered at 240 °C for 15 min [V].

Recently, alternative sintering methods have been developed to overcome some of the drawbacks related to conventional oven sintering (e.g. incompatibility with low-cost substrates, processing speed limitations, high energy consumption, etc.). These include laser sintering [57-61], pulsed light sintering [62-65], microwave sintering [66,67], chemical sintering [68-70], and plasma sintering [71], in addition to the RES [I-III] and SUFS [IV] methods introduced in this Thesis. The RES and SUFS methods are described in the following Chapters 4 and 5, respectively, and compared against the other sintering methods in Chapter 7.

4. Electrical Sintering

This Chapter presents the RES method high-lighting the main results of publications [I-III]. The method is demonstrated on inkjet printed silver nanoparticle structures by applying direct current (DC) voltage as well as via a near-field coupled alternating current (AC) electric field. The various applications of the method are summarized in Chapter 6.

4.1 Electrical Sintering with DC Voltage

Figure 9 illustrates a sintering setup, where sintering electrodes are in contact with the nanoparticle layer. When a voltage U is coupled between the sintering electrodes, a non-zero current flow (indicated by arrows in Figure 9) causes local heating in the layer. This initiates the sintering process and the structure undergoes a rapid transition in conductivity. The series resistor R_s limits the maximum current once the structure is sintered. Contact-mode electrical sintering has been applied using DC voltage in [I,II].

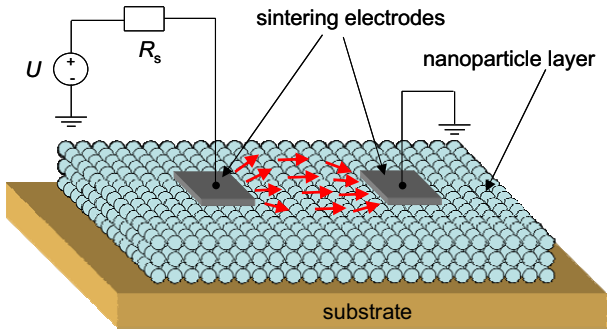

Figure 9. Schematic illustration (drawn out of scale) of a contact-mode electrical sintering setup [III].

4.1.1 Experimental Results

Figure 10 shows the measured response for RES of an inkjet printed test structure equivalent to that of Figure 5 with line dimensions $l \times w = 500 \times 60$ µm^2 [I]. The silver nanoparticle structure is rapidly sintered about 3 ms after applying U_{DC} as is evident from both the current I in Figure 10(a) and the resistance R_{tr} in Figure 10(b). The resistance of the sample decreases by more than four orders of magnitude during the process. The inset in Figure 10(b) reveals the timescale of the major transition to be less than 2 µs.

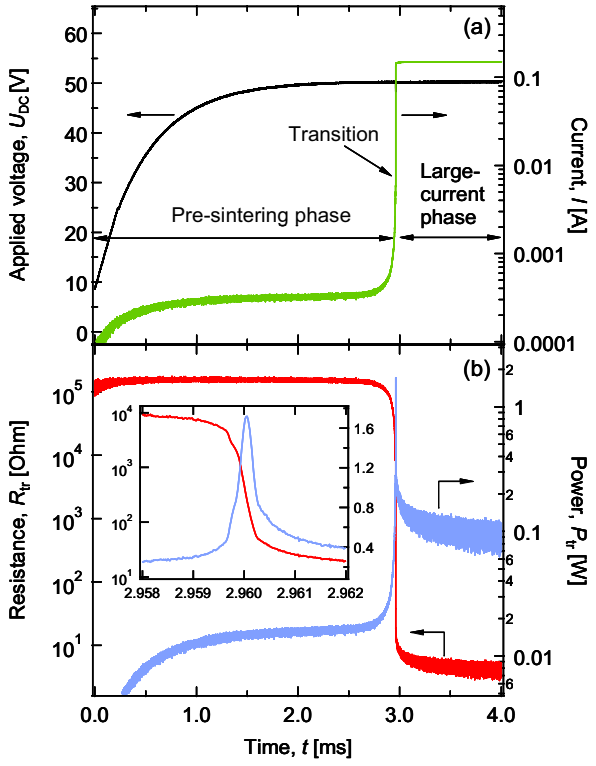

Figure 10. RES process as a function of time. (a) Voltage U_{DC} applied over the sample and the series resistor (R_S = 330 Ω), and the measured current I. (b) Sample resistance R_{tr} and dissipated power P_{tr}. [I]

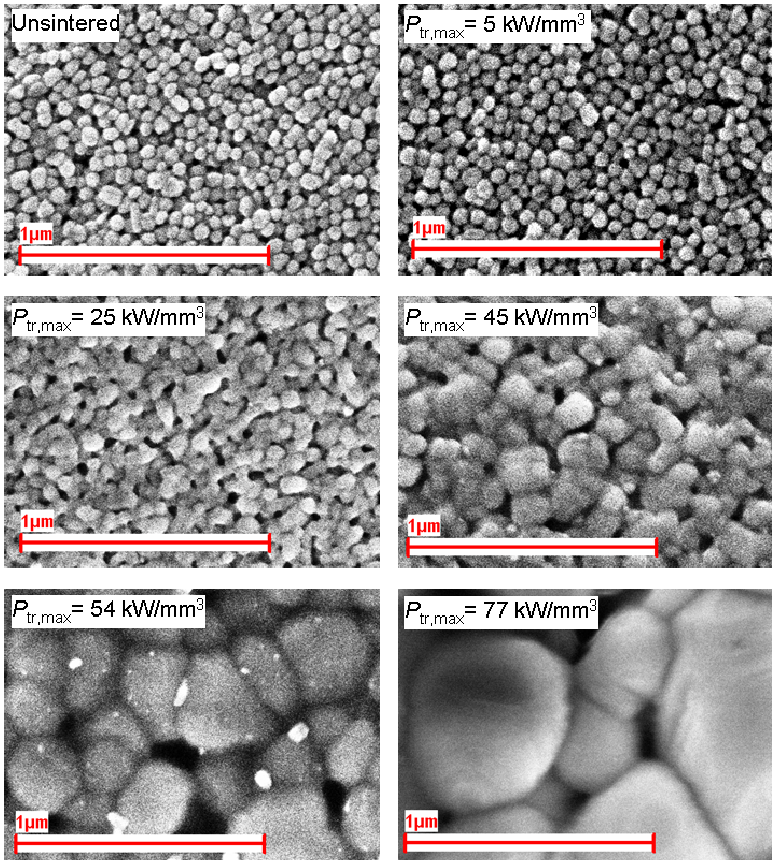

Figure 11. SEM images displaying progressive neck formation and grain-size growth as the maximum permitted peak power $P_{tr,max}$ of the RES process is increased [II].

The power dissipated in the nanoparticle structure P_{tr} peaks at the transition (Figure 10(b)). The peak power $P_{tr,max}$ strongly correlates with the efficiency of sintering, i.e., the resulting conductivity obtained [II]. In Figure 11, $P_{tr,max}$ is stepwise increased by adjusting the applied voltage U_{DC} and series resistance R_s accordingly. The SEM images of Figure 11 clearly display the interdependence between $P_{tr,max}$ and the resulting structural change with respect to the unsintered starting point.

4.1.2 Modeling

Classic sintering models based on mass transport between particles [112] fail to reproduce the fast dynamics observed for RES (see e.g. Figure 10). For the unsintered nanoparticle structure, where the minimum interparticle spacing is controlled by the thickness of the ligand shell (typically of the order 1 nm as shown in Figure 7(a)), thermal expansion can significantly affect the electro-thermal feedback process induced by the voltage boundary condition. Consequently, a new statistical model based on thermal expansion of the nanoparticles has been developed and compared with experiments [3].

In [3], a percolation model is adopted to simulate the randomness of the structure whereas the nanoparticles are assumed to be of equal size at any one moment during RES. As the particles expand under Joule heating, the average gap size is reduced, and increasingly more gaps are irreversibly decreased to zero to form a connected (percolating) system. Comparison with experimental results shows good agreement for the dynamics of the process [3]. In Figure 12, the temperature of the nanoparticle layer is estimated via simulations and measurements during the sintering process, where different emissivity values are applied for the infrared (IR) camera measurements before and after the transition [3].

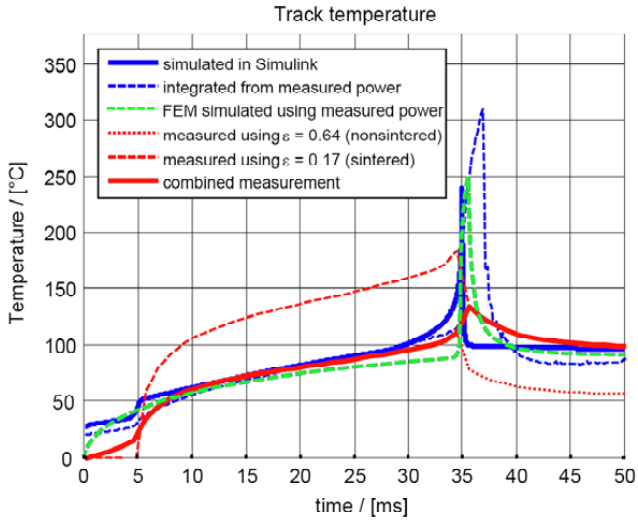

Figure 12. Simulated and measured temperature of nanoparticle layer during RES [3].

4.2 Contactless Electrical Sintering

Utilizing an AC electric field enables RES without physically contacting the nanoparticle structure. In [III], this is accomplished by applying sintering electrodes above the sample, which capacitively couple to the printed layer. The electrode geometry is arranged so as to provide an approximately homogeneous electric field across the unsintered structure. An adequate coupling reactance (at a feasible working distance between the sintering electrodes and nanoparticle layer) is obtained when operating at microwave frequencies.

Contactless RES surpasses many of the impracticalities associated with DC sintering; although DC RES provides excellent performance, contacting the layer limits processing speeds in many applications and is challenging when a large contact resistance is present between the electrode and the nanoparticle material. Furthermore, sintering large areas with DC voltage is problematic since the process easily leads to path formation (the electrical current cannot be directed to unsintered areas once a conducting route between the sintering electrodes has been formed).

4.2.1 Capacitive Coupling at Microwave Frequencies

The AC RES setup can be represented with a circuit comprising a Thévenin equivalent voltage source U_{Th} with impedance Z_{Th} and a load impedance Z_{L}, which is the equivalent of the impedance seen from the sintering electrodes. A major benefit of contactless AC RES over DC sintering is the possibility to prevent the short-circuit effect as explained in [III] using the circuit model of Figure 13. In Figure 13, we assume the nanoparticle structure to be divided into a set of parallel lines between the sintering electrodes, where R_{i} represents the line resistance and C_{s} the coupling capacitance between the line and the sintering electrodes. If

$$\frac{1}{\omega C_s} > R_i \tag{1}$$

for all R_i, and $\Im\{Z_{\mathrm{Th}}\} = -\Im\{Z_{\mathrm{L}}\}$ to tune out the coupling capacitance, the total power dissipated in the nanoparticle layer is [III]

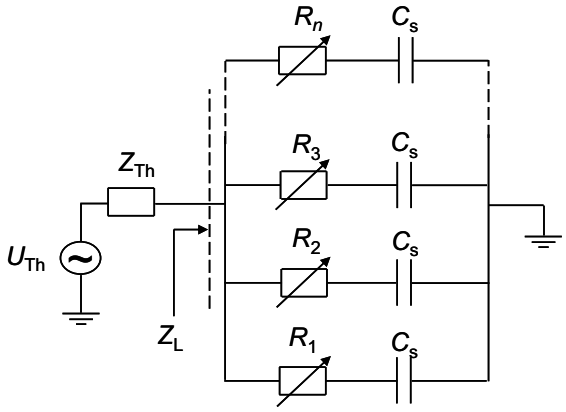

Figure 13. Equivalent circuit model for contactless RES of parallel lines [III].

$$P_L \approx \frac{\frac{R_{av}}{n}}{\left(\frac{R_{av}}{n} + R_{Th}\right)^2} \left|U_{Th}\right|^2, \tag{2}$$

where $R_{\mathrm{Th}} = \Re\{Z_{\mathrm{Th}}\}$ and

$$R_{av} = \sum_{i=1}^{n} \frac{R_i}{n}, \tag{3}$$

while the power dissipated in R_i is [III]

$$P_i \approx \frac{R_i}{R_{av}} \frac{P_L}{n} \tag{4}$$

with P_{L} from Eq. (2). Hence, by appropriately arranging the coupling capacitance so that Eq. (1) is valid, Eq. (2) and Eq. (4) show that (i) positive feedback in power insertion can be achieved (e.g. in the same way as for DC sintering in Figure 10) while (ii) the power is distributed among R_i so that most power is delivered to the location with highest resistivity. This analysis holds true also for the case of a continuous nanoparticle layer between the sintering electrodes provided that the electrode spacing is less than the thermal diffusion length in the layer [113].

4.2.2 Experimental Results

In [III], contactless RES is carried out by moving the sintering head over a printed nanoparticle layer or vice versa with a fixed head over a moving substrate. The sintering experiment of Figure 14 was carried out by sweeping a coaxial sintering head (based on a SubMiniature version A (SMA) connector) across a set of inkjet printed nanoparticle lines of varied widths (w) at 1 mm s^{-1} with the working distance fixed at 10 µm. The power reflected from Z_L was sampled using a network analyzer to enable online monitoring of the process as demonstrated in Figure 14.

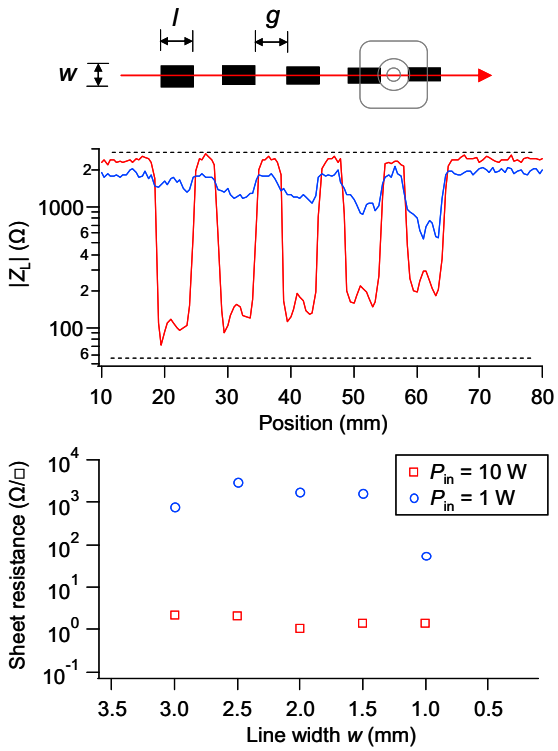

Figure 14. Contactless RES of silver nanoparticle lines inkjet printed on photopaper. The offline measured sheet resistance is in good agreement with $|Z_L|$ computed from the online measured reflected power. [III]

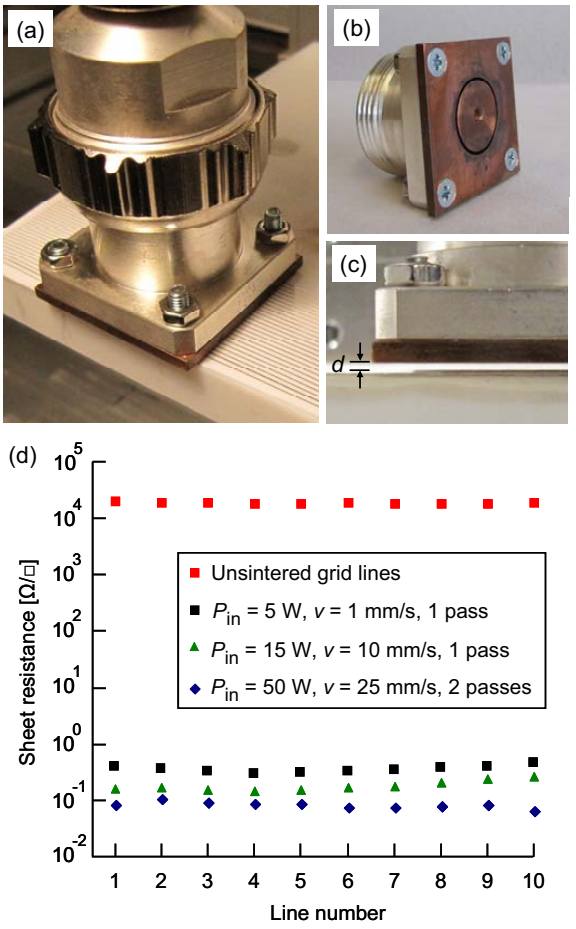

Figure 15. Contactless RES over an air gap ($d \approx 1$ mm) when RF power and sintering speed are varied. Coaxial electrode geometry providing large coupling electrodes and a small electrode spacing. [III]

The coaxial sintering head shown in Figure 15 is designed to fulfill the biasing conditions of Eq. (1) when coupled over an air gap of ca. 1 mm. Efficient sintering is obtained also at high processing speeds without notable deviations in line resistance. The experimental results of Figure 15 confirm that an increase in processing speed can be compensated by increasing the sintering power.

5. Substrate-facilitated Sintering

Nanoparticle sintering can be chemically triggered at room temperature. In this Thesis, this is accomplished with specialty coated substrates. Of particular interest is that this process also enables the effective interconnection of discrete components to printed structures on flexible substrates.

5.1 Sintering Mechanism

The SUFS method is based on the chemical removal of the nanoparticle stabilizing ligand through interaction with the coating layer of the printing substrate [IV]. Once the ligand-capping is removed, physical contact between the exposed particle cores is made possible. Nanoparticle sintering then progresses via diffusion and the release of surface energy as described in Chapter 3.2. The final conductivity level is reached on the time-scale of days as compared to the millisecond performance obtained with RES in Chapter 4.

Chemically induced room temperature sintering has previously been demonstrated on silver nanoparticles by dissolving the stabilizing ligand with methanol [70] or salts [69], or through charge neutralization [68,114]. In [68], silver nanoparticle dispersions were inkjet printed onto substrates containing a polycation solution to provide electrically conducting patterning with resistivity five times greater than the resistivity of bulk silver. The experimental work of [IV] demonstrating SUFS was carried out in parallel with that of [68] and was first reported in [10].

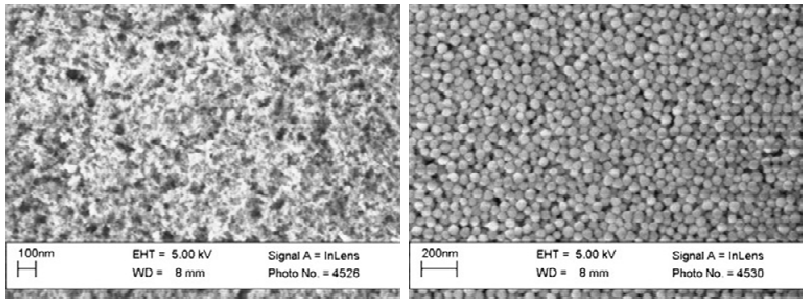

Figure 16. SEM images showing the structure of the silica-based ink-receptive coating layer on a reference substrate (left) and an optimal substrate providing room temperature sintering (right) [IV].

The ink-receptive coatings on inkjet substrates typically comprise a solvent absorbing layer and a surface layer providing particle fixation (see Figure 4(a) of Chapter 2.2). In [IV], it is shown that the coating layer of such a substrate can also provide in situ nanoparticle sintering at room temperature. Comparison between four commercially available inkjet substrates revealed substantial differences in the resulting conductivity of printed silver nanoparticle patterning even when all of the substrates were observed to have a silica-based coating layer (analyzed by Fourier-transform infrared spectroscopy (FT-IR) and energy-dispersive X-ray spectroscopy (EDX) SEM) [IV]. The SEM images of Figure 16 show the surface layer structure of an optimal substrate proving high conductivity via SUFS and a reference substrate. Although the analysis carried out in [IV] is not extensive enough to draw any conclusions as to whether a particular surface layer oxide structure is generally required to enable SUFS, it does suggest that the fixation mechanism with the reference substrates (for example that of Figure 16(a) having a porous, sponge-like appearance) is possibly more steric in nature as compared to the optimal substrates (which were found to have monodisperse oxide nanoparticles as the topmost layer as shown in Figure 16(b)) for which we can expect certain additives (e.g. the binder) to provide strong chemical affinity for the nanoparticle stabilizing ligand.

FT-IR spectra taken from the ink used in [IV] revealed the presence of carbonyl groups suggesting that the silver nanoparticles are coated with a polymer ligand such as the water-soluble polyvinylpyrrolidone (PVP). When the substrates were further analyzed using FT-IR it was found that the optimal coating

layers contain silanol groups [IV]. We conclude in [IV] that the silanol groups enable room temperature sintering by (i) dissolving the nanoparticle ligand by providing enhanced water absorption in the coating layer (as shown in [115]) and/or (ii) providing strong binding sites so that it is energetically favorable to detach the polymer ligands from the silver nanoparticles (the hydrogen bond between a silanol group and the carbonyl group of PVP is strong enough [116,117] to break the carbonyl–silver bond).

5.2 Experimental Results

The SUFS experiments of this Thesis were carried out on inkjet photopaper and transparency film substrates [IV]. Commercially available silver nanoparticle ink (DGP-45LT-15C from Advanced Nano Products Co. Ltd.) was inkjet printed onto the substrates at room temperature. All four of the test substrates provided fast solvent intake so that the patterning was dry to touch within a few minutes after printing.

Figure 17 shows the measured sheet resistance of lines printed on two reference substrates and a substrate with an optimal coating layer. The conductivity of the lines printed on the optimal substrate is around four orders of magnitude higher than obtained for the reference substrates [IV].

The effect moisture has on the sintering process was studied by inserting a set of samples into a controlled temperature/humidity environment (temperature held at 25 °C / relative humidity (RH) adjusted to 1-5 %, 30 % or 85 %) for three days prior to and one day after printing. The printing was carried out under ambient conditions (~ 50 % RH / 28 °C) within 3–5 min. The measurements were conducted one day after re-exposing the samples to ambient conditions.

Exposure to high RH enhanced the resulting conductivity as is evident from Table 1. The substrates with optimized coating layers provide conductivity around one-fourth of the bulk material when stored at high RH. The RH-dependent increase in conductivity was almost one order of magnitude for the opt. subs. 1 (a PET-based inkjet transparency film) and over two orders of magnitude for the opt. subs. 2 (a photopaper optimized for pigment-based inkjet inks). Even at low RH, the optimal substrates provide approximately three orders of magnitude higher conductivity than is obtained on the reference photopaper substrate. The RH dependence on conductivity affirms that water further facilitates the removal of the ligand, but exposure to high RH does not alone provide room temperature sintering. [IV]

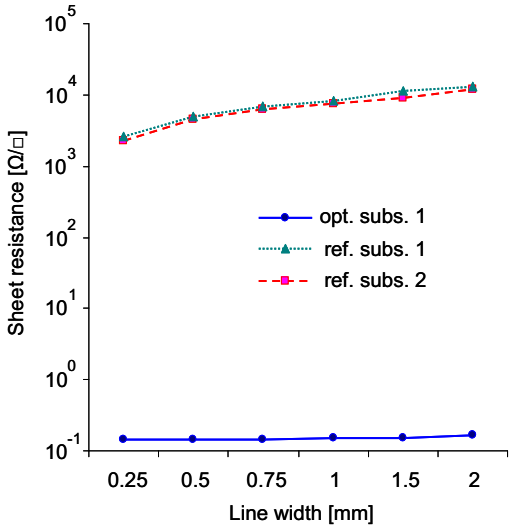

Figure 17. Measured sheet resistance of silver nanoparticle lines inkjet printed on coated substrates [IV]. The substrate with an optimal ink-receptive coating layer provides near bulk silver conductivity via SUFS at room temperature.

We expect that the SUFS process can be further improved from the level demonstrated in this Thesis via a better chemical match between the ink and substrate coating layer properties. Since sintering is triggered at the interface between the ink layer and substrate, this method provides an interesting possibility for dual-layer structures with an unsintered nanostructured top surface above a sintered highly conducting bottom layer. In Chapter 6.2, SUFS is utilized for attaching discrete components to printed conductors, where the sintered silver provides the metallic interconnects.

Table 1. Conductivity of silver nanoparticle patterning inkjet printed on coated substrates [S m^{-1} (% of bulk Ag)], when stored at different RH-levels before and after printing [IV].

RH (%)	Opt. subs. 1	Opt. subs. 2	Ref. subs.
<5	$1.0 \cdot 10^6$ (1.6 %)	$1.3 \cdot 10^5$ (0.2 %)	$3.7 \cdot 10^2$
30	$8.3 \cdot 10^6$ (13 %)	$1.9 \cdot 10^6$ (3.0 %)	$5.0 \cdot 10^2$
85	$1.7 \cdot 10^7$ (27 %)	$1.4 \cdot 10^7$ (22 %)	$1.2 \cdot 10^3$

6. Applications

This Chapter introduces various applications based on nanoparticle inks and the sintering methods developed in this Thesis. As demonstrated here, the conductivity level obtained by printing and sintering silver nanoparticles is sufficient for e.g. ultra high frequency (UHF) RFID antennas and enables low-resistance connector wiring between components. Conductor printing is required for practically all printed electronics systems including flexible displays, lighting panels, photovoltaics, keyboards, touch-screens, batteries, sensors, RF tags, memories, etc. A distinct advantage of the sintering methods developed in this Thesis is that they enable efficient sintering on temperature-sensitive substrates on which equivalent conductivity levels cannot be reached by conventional oven curing. Both methods provide energy-efficient processing and enable the use of low-cost, flexible substrates.

Also, an all-printed memory, where nanoparticle-based memory bits are written via RES with low voltage, is demonstrated. A contactless sweep-over approach is introduced for reading the information content of the memory. The SUFS method is shown to provide a novel approach for interconnecting discrete components to printed conductors. This approach can enable low-cost hybrid solutions combining silicon-based microchips with printed circuitry.

6.1 Printed Conductors

Compared to conventional printed circuit board (PCB) manufacturing, the potential benefits of printing as a technique for realizing electric circuitry include: (i) printing is a purely additive technique thus requiring significantly fever processing steps, (ii) the consumption of raw materials is reduced (can enable efficient use of expensive materials), (iii) printing enables the integration of components with diverse functionalities on the same substrate, (iv) provides fast turn-

around times with direct-write printing methods, and (v) the process can be more environmentally friendly (no corrosive etching chemicals required, reduced materials and energy usage) [17,92,118,119]. Metal nanoparticle inks [18,19,56,97,120,121] and metal-organic decomposition inks [122,123] are often employed since these provide higher conductivity than conducting polymers.

Figure 18(a) shows a typical interdigitated electrode layout that can be employed in e.g. a printed sensor. For example here, narrow and highly conducting finger electrodes are desired to provide high device efficiency. With efficient sintering methods, such as RES [I-III] and SUFS [IV] developed in this Thesis, this manufacturing approach becomes commercially attractive. Namely, the RES method enables processing speeds scalable to a R2R production line [III] while the exothermal SUFS approach eliminates the need for any external energy [IV]. Furthermore, both methods can also be selectively applied to certain parts of a printed structure. In Figure 18(b), for example, contactless RES has been applied using an AC probe to provide a narrow conducting path through a spin-coated layer of nanoparticles [I] (a similar effect as has been obtained in [59] with laser sintering).

Recent advances in solution-processed optoelectronic devices, e.g. OLEDs and thin-film PVs, make low-cost display, lighting and solar energy harvesting applications commercially viable [24,27,124,125]. However, the non-negligible sheet resistance of the transparent conductor causes a voltage drop along the electrode thus limiting the operation of practical, large-area devices. A simple and practical solution for reducing the effects of series resistance is to integrate a metal grid with the transparent conducting electrode (TCE) [126,127]. The optimal grid geometry is a trade-off between shadowing and resistive losses (contact resistance to the TCE and the resistance of the grid itself). Thus, high conductivity is essential for maximizing the device efficiency.

A typical OLED/PV device structure comprises a transparent substrate with a TCE for hole injection/extraction followed by the active layer(s) above which a low work function metal is evaporated as the cathode for electron injection/extraction. Figure 19(a) shows the layer sequence in this case with metal grid lines introduced between the substrate and the TCE. This device structure has been implemented in OLEDs for improving the homogeneity of brightness and reducing luminance loss [126,128] and in PVs for improving the power conversion efficiency [129,130]. As reported in [III], contactless RES has been demonstrated to provide efficient sintering of printed conductor grid lines at above 1 m min^{-1} processing speed on low-cost printing substrates.

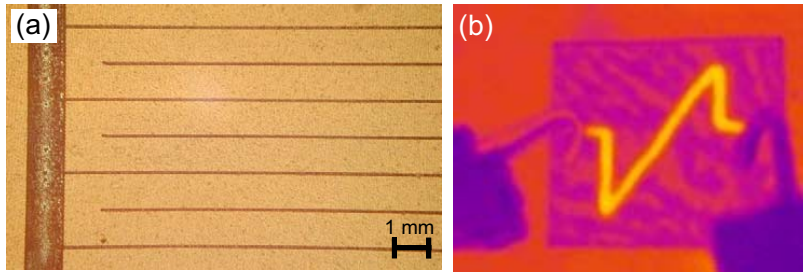

Figure 18. (a) Inkjet printed interdigital electrode structure (Harima NPS-J silver nanoparticle ink on Kapton polyimide substrate pre-treated with Novec EGC-1700). (b) Infrared image revealing a pulse-shaped conducting path formed by scanning an AC sintering probe over an unsintered layer of silver nanoparticles [I].

Alternatively, the layer sequence can be inverted (Figure 19(b)). The cathode is now the bottom electrode and there is no requirement for transparency of the substrate. In the inverted geometry, the metal grid is deposited as the final layer above the transparent electrode [131,132]. It is certainly not self-evident whether RES can be applied to grid lines printed on a conducting layer due to the screening effect of the TCE. However, also this approach has proven successful for a TCE with moderate (>100 Ω/□) sheet resistance: in this case, the TCE absorbs the RF power to generate heat instantaneously, which triggers the sintering process in the immediately adjacent silver nanoparticle grid lines. The grid lines shown in Figure 19(c) on indium tin oxide (ITO) coated glass (purchased from VisionTek Systems Ltd.) were inkjet printed and immediately sintered inline using the contactless RES setup of Figure 15. This procedure of applying grid lines over the TCE can similarly provide performance improvements for complementary thin-film photovoltaic technologies, e.g. copper indium gallium selenide (CIGS) and nanostructured titanium dioxide dye-sensitized solar cells (DSC) [133]. The possibility of applying a higher TCE sheet resistance provides cost-savings in manufacturing due to the reduced evaporation times required.

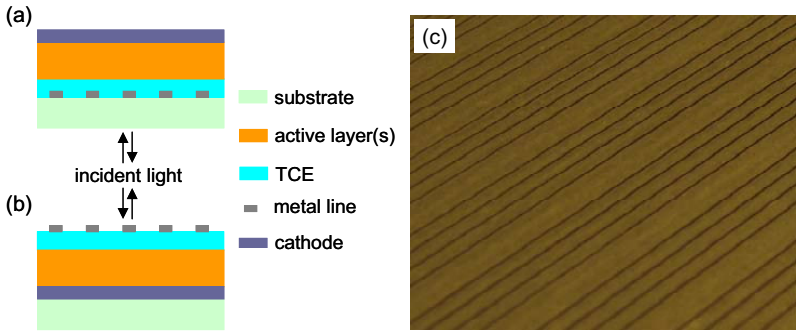

Figure 19. Schematic representation of an OLED / PV device structure with metal grid lines (a) directly on transparent substrate and (b) as topmost layer for the inverted layer sequence [III]. (c) Silver nanoparticle grid lines inkjet printed on ITO coated glass with 100 Ω/□ sheet resistance. The grid lines were sintered inline using contactless RES immediately after printing when in the ink was still wet.

6.2 Interconnects

Hybrid printed electronics, where discrete components (e.g. silicon-based microchips) are integrated with printed structures, offers a complementary approach to fabricating devices solely by means of printing. The possibility of interconnecting components to printed structures in a cost-effective manner significantly widens the scope of attainable applications and brings several printed electronics applications closer to commercial exploitation.

The transfer printing process has been demonstrated to make cost-effective use of silicon ICs by providing a method for placing extremely small and thin dice on flexible substrates [53]. When combined with an efficient interconnection procedure, this high-throughput assembly process can enable a multitude of low-cost applications, where various high-performance units on ultra-small silicon chips can be interconnected via printed circuitry.

The typical method used for attaching components to printed circuitry is flip-chip bonding (pick-and-place) [12] although other methods such as fluidic and vibratory assembly have been introduced [134]. The interconnecting bond is usually formed with a conducting adhesive [13]. However, recent studies have shown that silver nanoparticles provide high quality interconnects when sintered at sufficiently high temperatures [135,136]. In [35,36], silver nanoparticle ink is

inkjet printed to form interconnecting wiring between silicon chips and discrete passive components embedded face-up in the supporting substrate.

In this Thesis, the SUFS method is used for interconnecting discrete components to printed conductor wiring [IV]. The interconnection experiments were carried out by printing silver nanoparticle contact pads on the substrate and placing a discrete component on the pads when the ink was still wet. The ink is instantaneously absorbed into the substrate when the component is brought into contact and the SUFS process provides a high quality interconnect between the component electrodes and the printed wiring at room temperature.

In [IV], the contact resistance was roughly estimated by attaching surface-mount chip resistors to printed pads (as shown in Figure 20(a)) and measuring the resistance across the component. Here, the measured resistance was approximately 2 Ω above the nominal component resistance. In Figure 20(b), the interconnection method is demonstrated with a surface-mount light emitting diode (LED).

The component interconnection procedure developed in this Thesis is expected to enable efficient component assembly in both R2R and digital printing processes. Figure 20(a) provides an exemplary set-up, where components are attached to inkjet printed circuitry. Here, the placement accuracy is limited only by the accuracy of the printer's motorized stages.

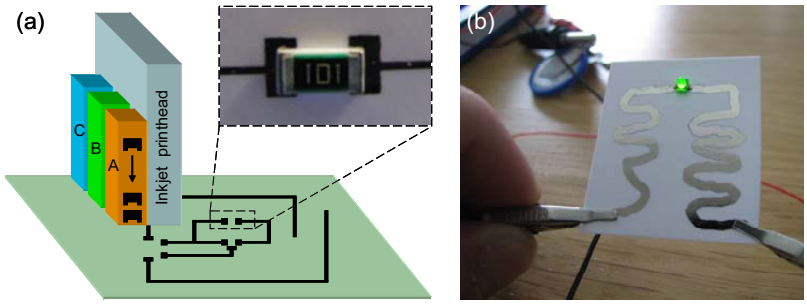

Figure 20. Component interconnection procedure based on the SUFS method. (a) Schematic illustration of a setup for drop-on-demand printing of circuit wiring and place-on-demand interconnection of discrete components. The method is demonstrated with surface-mount chip resistors attached to inkjet printed contact pads. (b) Surface-mount LED connected to wiring by placing the LED over still partially wet nanoparticle ink patterning. [IV]

In practice, an adhesive is required in order to increase the mechanical strength of the interconnection. The risk of shorting the printed pads when the component is attached can be minimized by using an anti-wetting agent such as a fluoropolymer between the component electrodes. In addition, the electrical contact could be further optimized by also applying a sintering agent on the component electrodes.

6.3 RFID Antennas and Wireless Resonant Tags

Metal nanoparticle inks and pastes can be used for printing antennas [37-39,V] and RF waveguides [137-140] with reasonable efficiencies. The majority of recently published work on printed antennas has concentrated on RFID and wireless local area network (WLAN) applications with operating frequencies in the HF (3 - 30 MHz) or UHF (0.3 - 3 GHz) bands. At HF, the operation is usually based on inductive coupling and coil antennas are used [34,50,141,V]. The reported antenna types for operation at UHF have included at least inkjet printed monopole [142], dipole [37,38,V] and patch [39,143] antennas.

RFID is a technology for automated identification of objects equipped with RFID tags [144]. A passive RFID tag has an antenna, a memory, circuitry for communicating the stored information to the reader via load modulation, and possibly other components, such as sensors. With the trend of RFID spreading from logistics to include consumer products, the IC, tag antenna manufacturing, and chip attachment processes are continuously developed to enable a low-cost implementation [134]. Printed silver nanoparticle ink antennas are unlikely to compete in price with antennas mass-produced by traditional copper or aluminum etching processes. However, the development of copper nanoparticle inks [97] and the preliminary work demonstrating potential for completely R2R printed HF RFID tags [50] make this manufacturing approach all the more appealing.

In this Thesis, RFID antennas were inkjet printed using commercially available silver nanoparticle ink onto Kapton polyimide film and subsequently sintered at 240 °C for 15 min to obtain conductivity approximately one-fourth that of bulk silver [V]. For HF coil antennas, the printing and sintering process was repeated to increase the conductor thickness above ca. 0.5 µm obtained for one printed layer. A tuning capacitor was attached to the coil and the measured frequency response was fitted to that of an equivalent circuit model. Q-values of 5.3 and 9.4 were obtained for the coils with layout shown in Figure 21(a) when

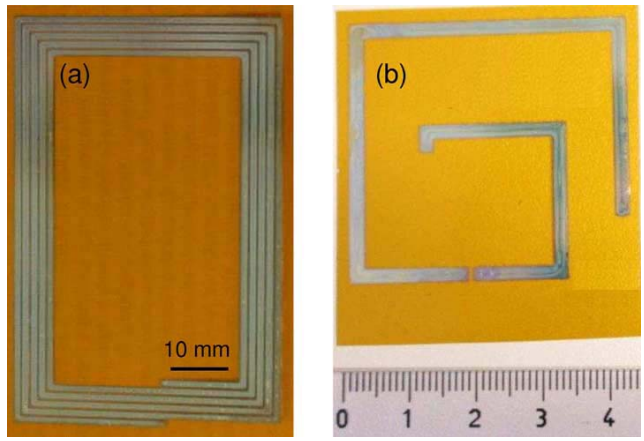

Figure 21. RFID antennas inkjet printed with silver nanoparticle ink. (a) Coil antenna targeted for operation at 13.56 MHz. (b) Spiral-shaped half-wave dipole antenna designed for direct impedance matching to a RFID microchip at 867 MHz. [V]

printed in two and three layers, respectively [V]. The Q-value provides a measure of the efficiency of the coil for coupling the transmitted energy to the microchip. Here, the inkjet printed coils with limited conductor thickness have higher losses compared to etched RFID coil antennas with Q-values typically around 30-80 [145].

UHF RFID tags are usually designed to operate in the far-field of the reader antenna. A passive tag extracts part of the incident RF power transmitted by the reader so that no external power source for the IC is required. The impedance matched tag antenna, which is in resonance at the frequency of the wavefront, has a large radar cross-section. Thus, part of the received power is reflected at the tag and detected by the reader. Communication from the tag to the reader is realized with backscatter modulation whereby appropriate switching of the input impedance of the microchip leads to a modulation of the signal that scatters back from the tag to the reader.[144]

The half-wave dipole antenna of Figure 21(b) was studied in [V] for evaluating the performance of nanoparticle ink for printing UHF RFID tag antennas. This (Palomar) antenna design is compact in size and provides efficient material usage [146]. Six prototype antennas, printed in one layer of ink, were characterized by measuring the antenna effective aperture and comparing the obtained

results to a reference etched copper antenna with a conductor thickness of 18 μm. The effective aperture is defined as the ratio of the power delivered to the load with respect to the power density of the incident wave at the tag location [147] and thus provides a descriptive measure of the performance of these power-limited passive tags. In [V], the effective aperture as a function of frequency was measured using the method of modulated backscattering described in detail in [148]. In addition, the reading distance was measured in a normal laboratory environment using a commercial RFID reader operating with 0.5 W RF power at 867 MHz. The maximum reading distance of the inkjet printed antennas was 3 m, while 5 m was recorded for the reference copper antenna [V].

The results of [V] thus indicate that metallic nanoparticle inks can enable printed UHF RFID tag antennas nearly equal in performance with traditional copper and aluminum tags whereas obtaining a low enough series resistance for the printed HF coil is challenging. While far-field UHF RFID antennas couple via electromagnetic waves (the antenna current forms a standing wave along the antenna conductors), the HF coil antennas need a long conduction distance to couple via the reactive magnetic field (here, the coil antenna and coupling distance are small compared to the wavelength and the coil current can be considered quasi-static).

For RF currents, the skin depth and proximity effects give rise to a non-uniform cross-sectional current distribution. In this work, for example, the effective coil resistance at the operating frequency (~ 13.56 MHz) was found to be approximately twice as large as the equivalent end-to-end measured DC resistance. Although the HF coil design can be somewhat optimized (e.g. by rounding sharp corners), applying thicker nanoparticle layers and an efficient sintering procedure are required to notably increase the voltage at the rectifier to provide longer reading distances. The radiation efficiency of UHF RFID antennas can be increased by optimizing the antenna design according to the current density distribution. In [38], for example, a thicker conductor layer was printed around the antenna feed point with highest current density. Similarly, a grid structure was applied in [149] to obtain an advantageous trade-off between electrical performance and material costs.

In addition to all-printed RFID tags, there is also interest for logic-free tags and wireless sensors, which are simple enough to be R2R printed at high web speeds without exhaustive process optimization and tuning. In this Thesis, a chipless inductively coupled RF resonant tag was printed and analyzed [VII]. A floating-bridge circuit layout was deployed to allow for possible registration

errors between the successive printed layers. Figure 22 shows a set of prototype tags R2R gravure printed using silver nanoparticle and dielectric inks. This circuit layout is similar to that of HF band electronic article surveillance (EAS) resonators. However, EAS is not considered to be among the targeted applications for printed RF tags mainly due to the limitations in conductor thickness and coil performance when printed in one layer [150]. A dual-band read-out approach is suggested in [VII] to enable activation or switching of the tag via an interlinking memory bit printed between one of the tuning capacitors and a capacitive grounding plate. As demonstrated in the following section, RES can be utilized to enable printed low-voltage-operated switches. The printed memory bit could also be replaced by a printed sensing element in order for the tag to function as a wireless sensor.

Figure 22. Wireless RF resonant tags R2R gravure printed using silver nanoparticle and dielectric inks[7].

[7] These RF tag prototypes were printed by Dr. H. Kang and colleagues at the Flexible Display Research Centre of Konkuk University in continuation of the work reported in [VII].

6.4 Memory

Whether an interactive board game, an electronic golf scorecard, or an RFID tag, many printed electronics applications require memory. Hitherto, various printable non-volatile electronic memory configurations have been demonstrated [40,41,151-154] and the first commercial printed memory products are currently entering the market [155]. The RES method developed in this Thesis lends itself as a printed WORM memory [4,5,156,VI].

In order to extract the information content from printed memory or sensor elements, some form of read-out is required. For example, a RFID microchip with a sensor interface can enable measuring a printed sensor and communicating the data via a printed antenna [46]. In [156], a computer-controlled programming / reading device is demonstrated for a RES-based memory. In this Thesis, a contactless read-out scheme is introduced and demonstrated for an inkjet printed memory based on silver nanoparticles [VI].

6.4.1 Low-voltage-operated All-printed Memory

The voltage and power levels for RES can be decreased from that originally demonstrated in [I] by scaling the sample dimensions accordingly [4]. The electrically programmable memory reported in [VI] was printed in two stages: a conducting base pattern was first printed in one session and small memory bits were printed afterwards as a separate processing stage. The complete memory was printed onto a transparent plastic film with an ink-receptive coating layer (equivalent to opt. subs. 1 in Chapter 5). The base electrode pattern was inkjet printed with ink containing polymer-capped silver nanoparticles in order to directly obtain high conductivity via SUFS at room temperature [IV] whereas an ink containing thiol-capped silver nanoparticles, which does not undergo spontaneous SUFS when printed on this substrate, was used for printing the memory bits. Hence, the initial (state “0”) bit resistance was typically above 10 kΩ [VI].
Figure 23(a) shows the measured bit resistance and switching voltage for a typical transition from state “0” to state “1” via RES. In [VI], the bit state was further switched from the low-resistance state “1” to an open-circuit state “2” by driving current through the bit (fuse-like action [156]) as shown in Figure 23(b). This memory concept provides low-voltage, two-state memory operation with below 100 ms switching times demonstrated.

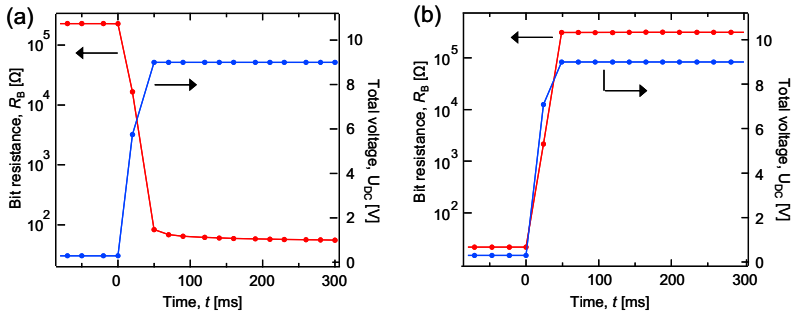

Figure 23. Measured bit resistance R_B and applied voltage U_{DC} during bit state switching. (a) Transition from the high-resistance state "0" to the low-resistance state "1" via RES. (b) Transition from state "1" to the open-circuit state "2" via bit burning (fuse-like action). [VI]

6.4.2 Contactless Read-out

The contactless read-out scheme of [VI] is based on capacitive coupling between the printed conductor patterning and the tip of a PCB. Here, the memory base pattern is arranged as a conducting comb of parallel lines adjacent to a common electrode. The memory bits, printed between the lines and the common electrode as schematically shown for one bit in Figure 24(a), modulate the electrical surface-area of the lines. The data is read-out by sweeping the PCB tip over the memory. In [VI], some of the lines are permanently interconnected to the common electrode for reference (closed bits).

The PCB tip employed in [VI] is structured from two coupling electrodes, A and B, and a large ground electrode. The voltage signal transferred from electrode A to electrode B with respect to ground is measured. Figure 24(b) shows the equivalent circuit model, where C_{INT}, C_1 and C_2 represent the internal capacitance between the electrodes A and B, and the coupling capacitance between each electrode and the line, respectively, while C_A, C_B and C_{GND} are the capacitances of the electrodes and the memory pattern with respect to the ground electrode. Figure 24(c) shows the simulated voltage transfer response as the PCB tip is swept over a 0.7 mm wide line terminated with an open (state "0" or "2") vs. closed (state "1") bit. The modulation of C_{GND} according to bit state is clearly visible in the read-out response.

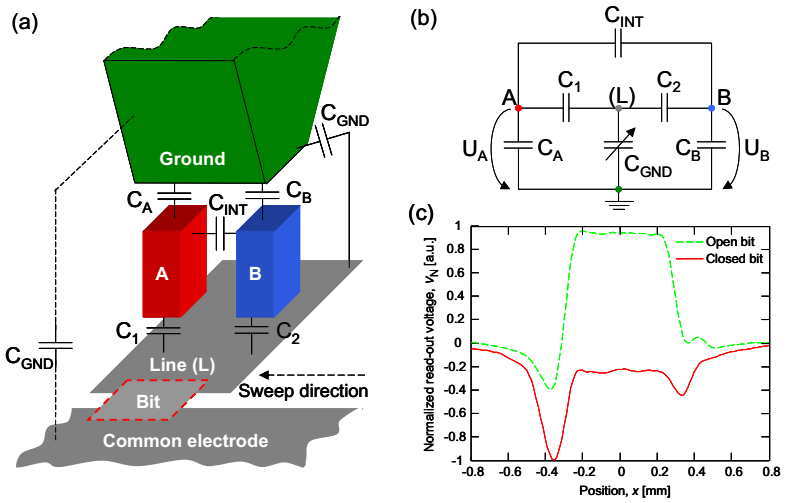

Figure 24. Setup enabling contactless sweep-over read-out of printed memory. (a) Schematic illustration of the coupling electrodes (A and B) at the tip of the PCB. (b) Equivalent circuit model. (c) Simulated read-out response for a single 0.7 mm wide line terminated with an open vs. closed bit. [VI]

Figure 25(a) shows the comb-like memory layout utilized in [VI] and Figure 25(b) the corresponding read-out response for the lines marked A-F. The reference lines B and D are terminated with closed bits, which remain permanently in state “1”. In sweep 1 of Figure 25(b), the bits connecting the lines A, C, E and F to the common electrode, are in the high-resistance state “0” and these lines induce positive-valued peaks in the read-out signal due to weak ground coupling. In sweep 2, the bits correspondent to lines A, E and F have been switched (via RES) to state “1”. This switch is visible in the read-out response as a change from high signal peaks to almost non-existent ripple about the null-level. In sweep 3, the memory bit joining line E to the common electrode is further switched from the low-resistance state “1” to the open-circuit state “2”. Now, the amplitude peak corresponding to line E has reappeared in the read-out signal. An unsintered bit can also be programmed directly from state “0” to state “2” as is demonstrated with line C in Figure 25. [VI]

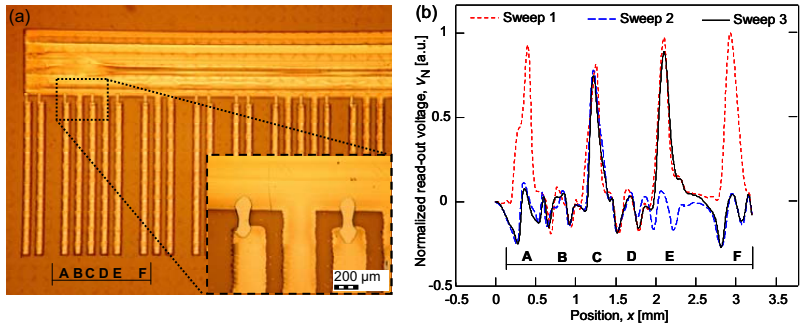

Figure 25. (a) Electrically programmable inkjet printed memory. Memory bits connecting the lines to the common electrode are shown in the inset. (b) Measured read-out response when the PCB tip is swept over the selected lines labeled A-F. In sweep 1, the bits corresponding to lines A, C, E and F are in state “0”. In sweep 2, lines A, E and F are short-circuited to the common electrode via state “1” bits. In sweep 3, line E is once again disconnected from the common electrode via a state “2” bit. The reference lines B and D remain connected to the common electrode via closed bits during all sweeps. [VI]

This read-out method does not require for the PCB tip to pass over the actual memory bits; instead, a crude alignment of the reader device to the lines is sufficient for sweep-over read-out. With this implementation, only a very small volume of the memory bit material joining the conducting lines to the common electrode is required. This read-out approach can, more generally, be applied also to printed sensors, for example. Also here, the significant benefit would be the small volume of sensing material printed. The demonstrated memory design offers potential for high-throughput R2R production.

7. Discussion

Printed electronics can significantly extend the application space addressed by conventional silicon-based electronics. Where high-speed R2R printing motivates for large volume manufacturing to enable low-cost[8] components and products, contactless direct-write printing methods can generate benefits due to design flexibility, customization and minimal usage of expensive materials. These methods are inherently suited for producing large area circuits which, often inevitably, imply long conductor distances. High conductivity is essential

---

[8] *The term "low-cost" is frequently used in the context of printed electronics. It can refer to the manufacturing cost per device or it can be associated with manufacturing line setup and maintenance costs, which can be significantly lower than with conventional semiconductor fabrication. At the low limit (a R2R mass-manufactured device exhibiting a low fill-factor pattern), the total manufacturing cost per device (including material, facility, operator, electricity etc. costs) can, in principle, be dominated by the cost of the substrate (where, for example, DuPont Teijin Melinex ST504 PET currently costs ca. \$3 m^{-2} at 125 µm film thickness, when purchased as a roll 300 mm in width and 475 m in length). Silver nanoparticle inks are currently priced at around \$5 - \$10 g^{-1} for a one-time purchase order of less than 1 kg and, according to one supplier, can go down to \$2 g^{-1} if purchased in very large quantities. As an example, inkjet printing with 10 pL drop volume and 20 µm dot pitch, as used in [V], equates to \$50 - \$250 m^{-2} for one printed layer. Hence, while a nanosilver printed grid pattern with a low fill-factor can be price-wise competitive for photovoltaic or lighting applications, the ink costs for RFID antennas can be less economic; using the large-quantity price estimate, the dipole and coil antennas of Figure 21 calculate roughly to \$0.01 and \$0.10 when printed in one and three layers, respectively.*

for reducing the total resistive losses and directly affects material costs by allowing the line widths and/or number of printed layers to be reduced. As is the case with printing methods, there similarly is no one particular sintering method which can perfectly address all of the numerous applications and associated production scenarios. The objective of this Chapter is to discuss and compare the RES and SUFS technologies to other sintering methods. An outlook on the future prospects of these technologies is also provided.

Different sintering methods rely on different physical mechanisms for coupling energy to the nanoparticle structure. Thermal ovens transfer energy via convection, conduction and thermal radiation so that the printed pattern and the substrate are heated alike. Usually, the temperature distribution within an oven is uniform and this sintering method can be described as being neutral in terms of feedback. Plasma sintering is similarly carried out using fixed process conditions and the sintering efficiency is strongly influenced by the energy level of the plasma interacting with the nanoparticles [71]. RES, as applied in this Thesis, exhibits strong positive feedback. Namely, the electric field applied across the nanoparticles induces current flow through the structure. This leads to local heating by dissipation, which increases the conductivity of the structure and further increases power dissipation via Joule heating. Microwave oven sintering relies on the same physical mechanism as RES for energy transfer, but allows significantly less control over biasing. Commercial microwave ovens typically comprise a magnetron source and a rectangular resonant cavity, where several modes can coexists. The resultant field pattern also depends on the size, shape and orientation of the printed sample, which can cause a notable perturbation to the field during sintering. Nonetheless, with sufficiently long sintering times and optimized target structures, sintering by microwave irradiation has been proven successful [66,67]. Laser sintering is employed by scanning a beam across printed patterning [60,61]. The wavelength of the laser can be tuned to obtain optimal energy coupling to the nanoparticle structure [57,58]. A very high-energy light pulse can be used sinter nanoparticles over a large area [62,64,65]. The adjustable parameters include pulse duration (typically in the range of 0.1 - 10 ms), intensity, impinging wavelengths and the number of pulses. With the operating parameters applied in [65], only the top surface of the printed silver nanoparticle track became efficiently sintered due to the photothermal effect leaving the inner part (lower half of the ca. 500 nm thick track) only partially sintered via the heat transferred from the surface. A major benefit of pulsed light sintering is the ability to sinter copper inks under ambient conditions without oxidation [62]. In

[63], laser and pulsed light sintering are classified as negative feedback methods due to the increase in reflectance of the target surface (decrease of energy coupling) during sintering. Indeed, the in situ reflection image of the laser is utilized in [58] to enable real-time monitoring of the sintering process. SUFS and other equivalent sintering methods [68-70,114] rely on a chemical reaction to detach the anchoring groups of the stabilizing ligands from the surfaces of the nanoparticles. Thereafter, the exposed nanoparticles sinter at room temperature through the release of stored energy as the total surface area of the nanostructured system is reduced.

Table 2 is an attempt to evaluate and compare the RES and SUFS methods against oven sintering, laser sintering, pulsed light sintering, microwave sintering and plasma sintering. The performance in terms of various criteria, and feasibility for certain methods of implementation, are graded on a relative scale as excellent ("++"), good ("+"), fair ("-"), or poor ("--"). Some data points are marked "N/A" (not available) to indicate that the literature on the use of the corresponding sintering method is limited, or non-existent, with regard to the evaluation parameter being compared. Although the ratings in Table 2 have been assigned according to the current knowledge and best understanding of the author, it must be emphasized that this comparison is not established upon any single comprehensive study undertaken using well-specified samples etc. Further to that, this ranking is more or less inextricably intertwined with the application in question and the manufacturing parameters used. For example, the energy-efficiency of oven sintering is related to the pattern fill ratio and the number of devices produced in one session. Nonetheless, Table 2 does provide a relatively unambiguous classification of the benefits and drawbacks of the various sintering methods, which are important to recognize when selecting a technology according to one's production needs.

In the first row of Table 2, the process speed is compared as per the duration of the transition from the initial unsintered state to the sintered state. Millisecond performance can be achieved with RES [I], laser sintering [57] and pulsed light sintering [62,64,65], whereas microwave sintering has been demonstrated on time-scales of 3-300 s [63,66]. One can argue that, in an ordinary microwave oven, an electric field strength equivalent to that enabling millisecond RES will unavoidably cause electrical breakdown through the nanoparticle layer (hence destroying the sample) due to the absence of proper biasing (as described in Chapter 4, the RES process is controlled by applying a power limiting resistor or by arranging an appropriate coupling capacitance). Oven sintering is typically

Table 2. Comparison of sintering methods with respect to selected evaluation parameters (Legend: “++” excellent; “+” good; “-“ fair; “--“ poor; “N/A” insufficient data).

Evaluation parameter	Oven	RES	SUFS	Laser	Pulsed light	Micro-wave	Plasma
Process speed	-	++	--	++	++	+	-
Flexibility regarding ink type and initial condition	++	-	--	+	N/A	-	-
Ability to process on temperature-sensitive substrates	--	+	++	+	+	N/A	N/A
Feasibility / readiness for implementing on R2R production line	+	-	++	-	++	-	--
Energy-efficiency[9]	--	+	++	+	-	-	-
Real-time process monitoring	--	++	--	+	N/A	--	--
Footprint of production tool	--	++	++	++	+	-	-
Capability for area-selective sintering	--	+	-	++	--	--	--
Maturity level (repeatability and predictability)	++	-	--	+	+	-	-

[9] Energy-efficiency is assessed here according to how well the process can direct and couple energy to printed features. A more informative evaluation would provide an estimate of the convertion efficiency between the energy the device draws from the mains supply and the energy delivered to the target structures for the purpose of sintering.

reported to require some 1-60 min [18,63,97,V] whereas plasma sintering was completed within 60 min in [71]. In [IV], we note that the final conductivity level is reached on a time-scale of days with the SUFS method. In fact, with SUFS tests equivalent to those carried out in [IV], the major transition in conductivity has been measured to occur already during the first 15 min after printing.

In this Thesis, RES is applied to silver nanoparticle structures printed onto coated paper [I-III] and plastic substrates [VI] as well as onto a non-absorbing plastic film, in which case, the nanoparticle layer is pre-dried to evaporate the ink solvent and to obtain the adequate level of initial conductivity required [III]. Similarly, also the recent studies on pulsed light, microwave and plasma sintering have been carried out on nanoparticle structures dried (in an oven or on a heated platen) prior to sintering [62,66,67,71]. Laser sintering has been successfully demonstrated not only on pre-dried nanoparticle layers [59,61], but also on wet ink directly after printing [57,58,60]. In Table 2, only oven sintering has been rated superior to laser sintering in terms of flexibility regarding ink type and initial condition; when neglecting external limiting factors (e.g. the thermal tolerance of the substrate) and oxidation etc. issues, one can assume that thermal oven sintering can deliver the required energy to evaporate the solvent and to detach the ligands irrespective of parameters such as particle size, solid loading ratio, initial conductivity and permittivity, and so on. Pulsed light sintering has not been assigned a grade on row two of Table 2 due to the fact that this technology has recently undergone significant advances in the commercial sector (the introduction of the PulseForge® line of products by NovaCentrix, Inc., for example) and the author is unaware of how wide a range of printed materials the method can ultimately be applied to. Sensitivity towards ink composition is currently recognized as a potential drawback of SUFS[10].

---

[10] *The printed memory introduced in [VI] and presented in Chapter 6.4 provides a practical example of how the chemistry and structure of the ink affect the sintering efficiency on a particular SUFS substrate. In this application example, it is desirable to have the counter-agent in the substrate coating layer provide high reactivity with one ink (used for printing the conducting electrodes) while demonstrating weaker interaction with the second ink type (used for printing the resistive memory bits later sintered via RES). Indeed, it is interesting to note that the SUFS-enabling counter-agent can, at least in principle, be optimized also in terms of selectivity over specific ink components.*

The ability to sinter nanoparticles on temperature-sensitive substrates is highly beneficial for printed electronics. At best, as is the case with chemical sintering (e.g. SUFS), both printing and sintering can be carried out at room temperature without any type of post-annealing. This way, conductors can be patterned not only on low-cost paper and plastic substrates, but also on textiles, over pre-existing features, and possibly even on biological surfaces such as on the leaves of plants if this was ever to be considered. RES, pulsed light and laser sintering similarly allow the use of temperature-sensitive substrates; with these methods, the temperature of the thin nanoparticle layer is raised only momentarily so that the heat leaked into the substrate remains at a tolerable level. For example, the pulsed light sintering simulations carried out in [64] suggest that the temperature of the silver nanoparticle layer exceeds 600 °C during irradiation and decreases to room temperature in less than a millisecond after the pulse (interestingly, a notably lower peak temperature is estimated for RES in Figure 12 [3]). Microwave and plasma sintering also couple energy selectively to the nanoparticle layer. However, since the literature found by the author on these methods fails to provide any record of the temperature profile during the process, these methods are not evaluated on row 3 of Table 2.

Typical R2R printing lines contain one or several curing ovens through which the web is guided after printing. Although incorporating an oven on a R2R production line is, as such, easy to implement, the oven lengths tend to increase to several meters in order to provide sufficiently long curing times for sintering. In addition to exhibiting a large tool footprint, large ovens are expensive, highly inefficient on energy usage and inflexible with respect to changing the temperature (lengthy response-times restrict online adjustment and the system is timely on start-up).

RES can enable contactless sintering at pass-over speeds exceeding 25 mm s^{-1}, but, in its current state of technological development, has not yet been implemented on a pilot-scale R2R line to demonstrate sintering of arbitrary printed patterning. The impedance seen from the coupling electrodes of the sintering head is a function of (i) the position and time-dependent sheet resistance of the nanoparticle layer, (ii) the pattern geometry, (iii) the electrical properties of the substrate, and (iv) the working distance. As discussed in [III], the optimal electrode geometry is, to some extent, a trade-off between feature resolution (the spacing between the electrodes should be smaller than the minimum individual printed features) and working distance (the distance between the sintering head and the web should be as small as possible to allow for the electric field between

the coupling electrodes to induce a lateral current through the unsintered layer of nanoparticles). In a practical R2R environment, a working distance of not less than ca. 100 µm should suffice to prevent significant deviations in impedance matching due to web fluctuations or substrate roughness [III]. Is this sense, a sintering electrode arrangement of the kind shown in Figure 15 can provide a working solution. One possibility for R2R RES would be to implement an array of such sintering heads across the width of the web. Efficient power coupling to the printed features would then be achieved via real-time adjustment of the impedance match (and/or operating frequency) of each branch individually or by integrating several rows of sintering heads, where each row is stepwise matched to the progressively increasing pattern conductivity [III]. Furthermore, the sintering power should be scaled with respect to the feature dimensions to have uniform sintering of large areas and narrow patterns alike. High-performance control circuitry and specialized computational algorithms are thus necessary if these functions are to be carried out at high web speeds[11]. Evidently, RES has much potential for use as a fast, energy-efficient, and multifunctional sintering method also in R2R production, but a considerable amount of engineering effort is still required before optimal performance can be achieved.

In Table 2, SUFS and pulsed light sintering are perceived to exhibit excellent feasibility for a R2R production line implementation; 1) ink-receptive substrate coatings are generally R2R printable and sintering takes place in situ after printing, 2) pulsed light sintering is applied over large areas from a large working distance. Although laser sintering can be applied on a R2R system, the scanning-

[11] *A cost estimate for a hypothetical R2R RES station compiled using off-the-shelf components works out somewhere around $10 thousand to $50 thousand. Selecting an operating frequency somewhere around 1-3 GHz is beneficial in terms of component availability and price due to the existence of various mobile systems operating in this frequency range. The microcontrollers, oscillators, amplifiers etc., associated with each individual sintering head, are assumed to be built onto a standard PCB. The uncertainty in cost increases for the high-power RF modules, i.e. the impedance tuners and the directional couplers; also these should preferably be compact in size but, at the same time, should provide low-loss performance. Further cost determinants include the mechanics, cooling, enclosure, etc. The details of the cost analysis are not included in this Thesis overview.*

based mode of operation does not appeal as the most feasible approach for high-throughput mass-production. Then again, the energy-efficiency of laser sintering can be better than that of pulsed light sintering because the focused laser beam can be scanned over selected features only. A microwave oven can, at least in principle, be incorporated on a R2R line by introducing exit slots at both ends of the microwave cavity. However, precautions need to be taken in order to limit radiation leakage through the wide slots. Whilst radiation leakage is obviously an issue also with AC RES, the contactless RES method is based on near-field coupling and propagating electromagnetic waves are never intentionally transmitted from the sintering head[12]. Plasma sintering requires a vacuum chamber and is thus considered incompatible for integration with a R2R printing system (existing R2R plasma treatment units require offline loading/unloading of the printing rolls).

RES is the only sintering method, which can provide real-time monitoring of the conductivity per se. This is highly advantageous not only for ensuring that sufficiently high conductivity is obtained, but also for controlling the process to sinter to a pre-defined target resistance. In [157], for example, Aerosol Jet printed strain gauges are sintered using a DC RES setup, where an electronic regulator module is employed to stop the current flow once the targeted electrical resistance is achieved. In this Thesis, real-time monitoring is demonstrated also with contactless AC RES. With AC sintering, however, the associated instrumentation and data analysis are more complex than in the DC case. The load impedance (the impedance seen from the coupling electrodes) can be monitored during the process by measuring both the magnitude and phase of the power reflected from the sintering head (as demonstrated in Figure 14). In [III], we explain how the load impedance can be determined also from the measured tuner input impedance by mapping over the tuner. However, this setup arrangement necessitates measuring/simulating the impedance parameters of the tuner through all the adjustable (position) combinations applied. Consequently, a more practical approach is to apply a dual directional coupler between the sintering

---

[12] *When applying 100 W feed power at 2 GHz, the maximum power density at one meter distance from the sintering head of Figure 15 was measured to be 130 mW m^{-2}. This corresponds to an equivalent isotropically radiated power (EIRP) of 1.6 W, which is in the same range as that permitted for cellular handsets.*

head and the tuner. This way, the incident power and the power reflected from the load can be measured separately thereby enabling the load power to be extracted. A relevant improvement to the procedure applied in [III] is that the power dissipated in the target nanoparticle structure can, in this case, be directly measured and disentangled from tuner losses without using pre-measured data or complex mathematics. Laser sintering is the only other method, in addition to RES, which has been shown to enable in situ process monitoring. Here, the reflection image of the laser beam from the nanoparticle target structure changes significantly upon sintering and thus provides a means for qualitative analysis of the sintering degree in real time [58]. In Table 2, oven sintering, SUFS, microwave and plasma sintering are considered incapable of facilitating in situ monitoring of the sintering process. The high-energy light pulse reflection from the nanoparticle pattern could be imaged (after filtering) to possibly enable real-time monitoring of the process, but seeing that there is no record of such analysis in the literature, the pulsed light sintering method is left unevaluated on row 6 of Table 2.

Direct-write printed nanoparticle structures are usually sintered offline after the whole layer has been patterned. Nonetheless, many of the evaluation parameters already discussed above (process speed, ability to process on temperature-sensitive substrates, etc.) are equally important when performing sintering offline. The concept of integrating an inline sintering tool with a direct-write printhead undoubtedly inspires much interest. A vital parameter, in this case, is the footprint of the tool. It certainly appears feasible to have one or several laser beams follow the printhead so as to enable laser sintering on the fly (in a similar fashion as is carried out in [57,58]). Also contactless RES can potentially be applied using a small-scale device configuration. One feasible approach could be to incorporate a wide sintering card (something similar to the PCB sintering head of [III], but with larger coupling electrodes to increase the working distance) adjacent to a multi-nozzle printhead to provide in situ sintering on an industrial-scale inkjet printer. Although pulsed light sintering is best suited for large-area processing, it would seem reasonable to have a flash lamp system of this kind incorporated also on a direct-write printing system. SUFS is certainly compatible with direct-write printing (no additional post-treatment tooling required for sintering on the pre-coated substrates).

Laser lends itself readily to area-selective sintering; a focused laser beam is used in [59] to sinter inkjet printed and pre-dried gold nanoparticle structures at very high resolution (the sintering line width can go down to 1-2 μm). Further-

more, these laser processing tools can also be used for ablation [113] (e.g. for trimming of the printed features and for drilling via holes). In [I], we provide a proof-of-concept demonstration of area-selective RES by scanning an RF probe across an unsintered nanoparticle layer (Figure 18(b)). The experimental results presented in [I] are quite promising and there is undoubtedly much room for improvement; one possible approach to increase the sintering resolution could be to apply pulsed (instead of continuous) RF power in order to reduce thermal diffusion outside the targeted areas. Recent, though not yet published, experiments show that the SUFS substrates can be locally "activated" by jetting a counter-agent solution over selected regions on the coated substrate - thus, in principle, enabling area-selective sintering.

Oven sintering is by far the most mature of the sintering methods compared in Table 2. Also laser and pulsed light sintering are, in their current stage of development, estimated to provide better repeatability and predictability than RES, SUFS, microwave and plasma sintering. SUFS represents an immature sintering technology somewhat retarded by the limited understanding of the process (the underlying chemistry for explaining the susceptibility to environmental conditions has not yet been accurately characterized, for example [IV]). Nonetheless, as is clearly evident from Table 2, the methods developed in this Thesis feature many benefits and have the potential to become widely applied in printed electronics. The success and adoptability of RES will ultimately depend on how well the design and operating parameters are identified, and to what level these process variables can be controlled, optimized and automated. In fact, RES can potentially provide a generic tool for curing printed materials; the contactless RES setup of this Thesis has already been demonstrated to enable rapid and efficient drying of screen printed silver paste, for example. From a commercial aspect, the breakthrough sintering technologies are likely to become established as those which best serve the production requirements associated with certain "killer applications" yet to emerge in the printed electronics market. Hence, the production process may require sintering under an inert atmosphere (wherein plasma sintering could turn out to be most suitable) or e.g. sintering a low fill-factor pattern over a large area (in which case RES or laser sintering would presumably be the best choice in terms of manufacturing cost-efficiency).

The RES and SUFS methods are exploited in several of the applications studied in this Thesis. An advantageous feature of RES is that the process parameters (the required voltage and power) are scalable in proportion to the dimensions of the target structure. This dependency is exploited in the printed memory of this

Thesis, but also various other low-power application possibilities exist. One could imagine having various kinds of electronic circuits embedded in printed media, which carry out some function when activated by the end-user. Here, a hand-held contactless RES device could be employed to selectively sinter nanoparticle-based switches interlinking the circuits to a printed battery, for example.

A major drawback of the RES-based memory is the fact that the sintering process is irreversible. Furthermore, the viability of this memory technology is, to some extent, challenged by the long-term stability of the memory bits in their unsintered state (retention times above 100 days were reported in [4] for bits stored at low relative humidity). In some cases, the memory bits need to be pre-sintered to obtain initial resistance values within a desired range. Nevertheless, the fact that this memory structure is extremely simple, and each memory bit requires only a minimal volume of ink, does motivate to use this technology in certain memory applications (e.g. electronic fairground or car wash tickets, where each "ride" is irreversibly written into the memory until the ticket is used up). Recently, the RES WORM memory was implemented in a pilot-scale technology demonstration, where a thousand electronic questionnaire cards were produced for the Best Booth voting at Printed Electronics Europe 2011 Conference in Dusseldorf, Germany. The memory bits (for storing the information input by the user, i.e. the vote) were R2R flexo-printed at VTT using silver nanoparticle ink.

The memory bit resistance can be lowered also in a stepwise manner to enable multi-state operation [156]. The significant benefit here is the large data storage capacity (number of combinations) obtained with only a few printed memory bits. Evidently, the optimal memory configuration is a trade-off between the bit stability, the resolution of the reader, and the maximum available surface-area assigned for the memory layout. Even in light of the rather promising results obtained thus far, the aforementioned reliability-related issues are nevertheless to be overcome before this memory technology can become widely accepted. Even then, this is probably not the best solution for applications required to provide exceptional durability and life-time.

A first proof-of-concept demonstration of SUFS-enabled component attachment is reported in this Thesis. Although a more thorough investigation of the contact resistance and the repeatability of the process, as well as the environmental stability and mechanical durability of the interconnection, is yet to be carried out, the initial results are extremely encouraging; even after two years of shelf storage, the SUFS-interconnection to the surface-mount LED of

Figure 20(b) was still fully functional and did not degrade during routine handling. This confirms that it is certainly the sintered metal that provides also the mechanical connection rather than any kind of capillary effect in the substrate-ink-component interface.

The future potential of this component interconnection method is largely dependent on the resolution the process can reach. Minimizing the chip size complicates the assembly process and translates into ever narrower contact electrode spacing. Although the printing resolution obtained with e.g. inkjet systems is continuously increasing, the alignment accuracy of placing the chip over the printed contact areas is critical for the assembly procedure to be successful. Furthermore, the timing between printing the nanoparticle electrodes on the SUFS substrate and placing the component over the still partially wet ink, requires systematic control and optimization especially if several components are attached in parallel.

Wireless communication between printed electronics and external devices is an interesting topic of research and is expected to inspire disruptive solutions departing from standard technologies and protocols. The contactless read-out scheme introduced and demonstrated in this Thesis is a prime example of such a solution, which enables RF data transfer from the printed memory to the reader while allowing for remarkably unsophisticated printed circuitry. Contactless read-out of printed memory is beneficial in terms of reliability (circumvents e.g. contamination problems manifested in contact-mode read-out) and ease of use, and allows for the complete encapsulation of the memory with a protective film in order to extend the shelf life. Furthermore, the coupling electrodes and memory layout dimensions can be adjusted to enable read-out through a thicker packaging material (without line-of-sight) if required.

8. Conclusions

In this Thesis, nanoparticle sintering methods and applications for printed electronics were developed. The research work was carried out in a laboratory environment using commercially available materials. The majority of the test structures studied were fabricated by inkjet printing. R2R gravure printing was investigated for printing multilayer passive electric circuitry.

The research work of publications [I,II] addressed the problem of sintering nanoparticle structures on temperature-sensitive surfaces/substrates by introducing the RES method. RES was demonstrated to provide efficient and extremely fast sintering of inkjet printed silver nanoparticles, when performed by coupling a DC voltage over the structure. Publication [III] is a record of the work undertaken with the objective of developing the RES method towards a practical adaption suitable for e.g. printed electronics manufacturing. In [III], contactless RES was implemented by coupling the near-field electric field of a sintering head across the underlying nanoparticle layer. The biasing conditions allowing for controlled power delivery to the layer were derived and implemented at microwave frequencies. A completely different sintering approach is described in publication [IV], where printed silver nanoparticles underwent spontaneous room temperature sintering when printed on chemically matched ink-receptive surfaces. This SUFS method was demonstrated also to provide an efficient method for attaching discrete components to printed conductors.

The work carried out in publication [V] showed that UHF RFID antennas fabricated by silver nanoparticle printing and sintering can be nearly equal in performance with the traditional etched copper and aluminum tag antennas whereas obtaining low enough series resistance for inkjet printed HF coils can require multilayer printing. In publication [VI], an all-printed memory providing two-state operation via RES and fuse-like action was demonstrated. The memory was arranged as a comb pattern with the small memory bits interlinking conducting

lines and a large common electrode. The lines and common electrode were inkjet printed with polymer-capped silver nanoparticles to obtain high conductivity via SUFS on the (coated) plastic substrate whereas thiol-capped nanoparticles were used for printing the memory bits. The bit state data was read-out by sweeping a prototype reader over the memory. The capacitive modulation read-out method presented in [VI] can be utilized for low-cost memory applications as well as printed sensors. A passive RF resonant tag fabricated by R2R gravure and inkjet printing was studied in [VII]. The floating-bridge circuit layout lends itself to high-throughput manufacturing by allowing for registration errors between the successively printed conducting and dielectric layers. A multi-state tag concept was suggested in [VII] where the tags resonance frequency is switched from one frequency band to another by RES.

The example structures and materials studied in this Thesis by no means represent an exhaustive record of the possible applications enabled by these technologies. In fact, the RES and SUFS methods may also find use in applications outside the context of low-cost printed electronics, for example, in the textile industry or in the manufacturing of high-end products such as mobile devices. What is for certain is that printed electronics is, at least from an academic perspective, an extremely exiting, multidisciplinary field of research expedited by scientific advances made in e.g. self-assembly processes, carbon nanotube and graphene based materials engineering, and even molecular electronics. It will be interesting to see what role, if any, the sintering methods and/or applications presented in this Thesis will play in future printed electronics manufacturing or applications.

References

[1] M. Allen, A. Alastalo, M. Aronniemi, T. Mattila, K. Sääskilahti, M. Suhonen, and H. Seppä, "R2R Electrical Sintering of Nanoparticle Structures," *Proceedings of the 1st International Conference on R2R Printed Electronics*, Seoul, South Korea: 2008, pp. 291-296.

[2] M. Allen, M. Suhonen, J. Leppäniemi, A. Alastalo, T. Mattila, A. Kemppainen, and H. Seppä, "Electrical Sintering of Conductor Grids for Optoelectronic Devices," *Proceedings of LOPE-C*, Frankfurt, Germany: 2010, pp. 32-36.

[3] A.T. Alastalo, H. Seppä, J.H. Leppäniemi, M.J. Aronniemi, M.L. Allen, and T. Mattila, "Modelling of nanoparticle sintering under electrical boundary conditions," *Journal of Physics D: Applied Physics*, vol. 43, Dec. 2010, p. 485501.

[4] J. Leppäniemi, M. Aronniemi, T. Mattila, A. Alastalo, M. Allen, and H. Seppä, "Printed WORM Memory on a Flexible Substrate Based on Rapid Electrical Sintering of Nanoparticles," *IEEE Transactions on Electron Devices*, vol. 58, 2011, pp. 151-159.

[5] H. Seppä and M. Allen, *Method for manufacturing conductors and semiconductors*, Patent FI 121562 / US 2009301769 (Priority date: Jul. 21, 2006). 2009.

[6] M. Allen, T. Mattila, A. Alastalo, and H. Seppä, *Method and apparatus related to nanoparticle systems*, Patent FI 122014 / US 2009016924 (Priority date: Jun. 8, 2007). 2011.

[7] T. Mattila, A. Alastalo, M. Allen, and H. Seppä, *Electronics module, method for the manufacture thereof and applications*, Patent FI 122011 / US 7,915,097 (Priority date: Jun. 8, 2007). 2011.

[8] T. Mattila, A. Alastalo, M. Allen, and H. Seppä, *Method for producing conductor structures and applications thereof*, Patent FI 20075430 / US 7,759,160 (Priority date: Jun. 8, 2007). 2010.

[9] T. Mattila, A. Alastalo, M. Allen, and H. Seppä, *Structures based on nanoparticles and method for their fabrication*, Patent FI 122009 / US2009081431 (Priority date: Jun. 8, 2007). 2011.

[10] M. Allen, J. Leppäniemi, and T. Mattila, *Method and products related to deposited particles*, Patent appl. FI 20096179 (Priority date: Nov. 13, 2009). 2009.

[11] M. Allen, A. Alastalo, M. Aronniemi, J. Leppäniemi, T. Mattila, and H. Seppä, *Programmable printed electric code and programming device*, Patent appl. FI 20096341 (Priority date: Dec. 16, 2009). 2009.

[12] J. Lenkkeri, S. Kivelä, E. Juntunen, T. Jaakola, K. Nummila, M. Allen, T. Kaskiala, G. Hillmann, and A. Mathewson, "Development of Chip to Antenna Interconnections for Contact-less Smart Card Applications," *Proceedings of EMPC*, Oulu, Finland: 2007, pp. 472-477.

[13] J. Lenkkeri, T. Jaakkola, M. Lahti, M. Allen, and T. Kaskiala, "Chip/Antenna Interconnections for Contact-less Smart Card Applications," *Proceedings of the IMAPS Nordic Annual Conference*, Helsingor, Denmark: 2008, pp. 197-202.

[14] A. MacDiarmid, "Nobel Lecture: 'Synthetic metals': A novel role for organic polymers," *Reviews of Modern Physics*, vol. 73, Sep. 2001, pp. 701-712.

[15] A.R. Brown, A. Pomp, C.M. Hart, and D.M. de Leeuw, "Logic Gates Made from Polymer Transistors and Their Use in Ring Oscillators," *Science*, vol. 270, Nov. 1995, pp. 972-974.

[16] V. Subramanian, J.M.J. Frechet, P.C. Chang, D.C. Huang, J.B. Lee, S.E. Molesa, A.R. Murphy, D.R. Redinger, and S.K. Volkman, "Progress Toward Development of All-Printed RFID Tags: Materials, Processes, and Devices," *Proceedings of the IEEE*, vol. 93, Jul. 2005, pp. 1330-1338.

[17] J. Perelaer, P.J. Smith, D. Mager, D. Soltman, S.K. Volkman, V. Subramanian, J.G. Korvink, and U.S. Schubert, "Printed electronics: the challenges involved in printing devices, interconnects, and contacts based on inorganic materials," *Journal of Materials Chemistry*, vol. 20, 2010, pp. 8446-8453.

[18] D. Kim and J. Moon, "Highly Conductive Ink Jet Printed Films of Nanosilver Particles for Printable Electronics," *Electrochemical and Solid-State Letters*, vol. 8, 2005, p. J30-J33.

[19] S.B. Fuller, E.J. Wilhelm, and J.M. Jacobson, "Ink-jet printed nanoparticle microelectromechanical systems," *Journal of Microelectromechanical Systems*, vol. 11, 2002, pp. 54-60.

[20] M. Härting, J. Zhang, D.R. Gamota, and D.T. Britton, "Fully printed silicon field effect transistors," *Applied Physics Letters*, vol. 94, 2009, p. 193509.

[21] K. Hecker, ed., *OE-A Roadmap for Organic and Printed Electronics*, 3rd ed., VDMA Verlag GmbH, 2009.

[22] T.R. Hebner, C.C. Wu, D. Marcy, M.H. Lu, and J.C. Sturm, "Ink-jet printing of doped polymers for organic light emitting devices," *Applied Physics Letters*, vol. 72, 1998, pp. 519-521.

[23] M. Tuomikoski, R. Suhonen, M. Välimäki, T. Maaninen, A. Maaninen, M. Sauer, P. Rogin, M. Mennig, S. Heusing, J. Puetz, and M.A. Aegerter, "Manufacturing of polymer light-emitting device structures," *Proceedings of the SPIE*, 2006, p. 619204.

[24] P. Kopola, M. Tuomikoski, R. Suhonen, and A. Maaninen, “Gravure printed organic light emitting diodes for lighting applications,” *Thin Solid Films*, vol. 517, Aug. 2009, pp. 5757-5762.

[25] T. Aernouts, T. Aleksandrov, C. Girotto, J. Genoe, and J. Poortmans, “Polymer based organic solar cells using ink-jet printed active layers,” *Applied Physics Letters*, vol. 92, 2008, p. 033306.

[26] C.N. Hoth, S.A. Choulis, P. Schilinsky, and C.J. Brabec, “High Photovoltaic Performance of Inkjet Printed Polymer:Fullerene Blends,” *Advanced Materials*, vol. 19, Nov. 2007, pp. 3973-3978.

[27] A.C. Mayer, S.R. Scully, B.E. Hardin, M.W. Rowell, and M.D. McGehee, “Polymer-based solar cells,” *Materials Today*, vol. 10, 2007, pp. 28-33.

[28] H. Sirringhaus, T. Kawase, R.H. Friend, T. Shimoda, M. Inbasekaran, W. Wu, and E.P. Woo, “High-Resolution Inkjet Printing of All-Polymer Transistor Circuits,” *Science*, vol. 290, Dec. 2000, pp. 2123-2126.

[29] H. Yan, Z. Chen, Y. Zheng, C. Newman, J.R. Quinn, F. Dötz, M. Kastler, and A. Facchetti, “A high-mobility electron-transporting polymer for printed transistors.,” *Nature*, vol. 457, Feb. 2009, pp. 679-687.

[30] M.M. Voigt, A. Guite, D.-Y. Chung, R.U.A. Khan, A.J. Campbell, D.D.C. Bradley, F. Meng, J.H.G. Steinke, S. Tierney, I. McCulloch, H. Penxten, L. Lutsen, O. Douheret, J. Manca, U. Brokmann, K. Sönnichsen, D. Hülsenberg, W. Bock, C. Barron, N. Blanckaert, S. Springer, J. Grupp, and A. Mosley, “Polymer Field-Effect Transistors Fabricated by the Sequential Gravure Printing of Polythiophene, Two Insulator Layers, and a Metal Ink Gate,” *Advanced Functional Materials*, vol. 20, Jan. 2010, pp. 239-246.

[31] E. Gracia-Espino, G. Sala, F. Pino, N. Halonen, J. Luomahaara, J. Mäklin, G. Tóth, K. Kordás, H. Jantunen, M. Terrones, P. Helistö,

H. Seppä, P.M. Ajayan, and R. Vajtai, “Electrical transport and field-effect transistors using inkjet-printed SWCNT films having different functional side groups.,” *ACS nano*, vol. 4, Jun. 2010, pp. 3318-3324.

[32] H.-Y. Tseng and V. Subramanian, “All inkjet-printed, fully self-aligned transistors for low-cost circuit applications,” *Organic Electronics*, vol. 12, Feb. 2011, pp. 249-256.

[33] A. de la Fuente Vornbrock, D. Sung, H. Kang, R. Kitsomboonloha, and V. Subramanian, “Fully gravure and ink-jet printed high speed pBTTT organic thin film transistors,” *Organic Electronics*, vol. 11, Dec. 2010, pp. 2037-2044.

[34] D. Redinger, S. Molesa, S. Yin, R. Farschi, and V. Subramanian, “An Ink-Jet-Deposited Passive Component Process for RFID,” *IEEE Transactions on Electron Devices*, vol. 51, Dec. 2004, pp. 1978-1983.

[35] V. Pekkanen, M. Mäntysalo, K. Kaija, P. Mansikkamäki, E. Kunnari, K. Laine, J. Niittynen, S. Koskinen, E. Halonen, and U. Caglar, “Utilizing inkjet printing to fabricate electrical interconnections in a system-in-package,” *Microelectronic Engineering*, vol. 87, Nov. 2010, pp. 2382-2390.

[36] J. Miettinen, V. Pekkanen, K. Kaija, P. Mansikkamäki, J. Mäntysalo, M. Mäntysalo, J. Niittynen, J. Pekkanen, T. Saviauk, and R. Rönkkä, “Inkjet printed System-in-Package design and manufacturing,” *Microelectronics Journal*, vol. 39, Dec. 2008, pp. 1740-1750.

[37] L. Yang, A. Rida, R. Vyas, and M.M. Tentzeris, “RFID Tag and RF Structures on a Paper Substrate Using Inkjet-Printing Technology,” *IEEE Transactions on Microwave Theory and Techniques*, vol. 55, Dec. 2007, pp. 2894-2901.

[38] J. Siden, M.K. Fein, A. Koptyug, and H.-E. Nilsson, “Printed antennas with variable conductive ink layer thickness,” *IET Microwaves, Antennas & Propagation*, vol. 1, 2007, pp. 401-407.

[39] M. Mäntysalo and P. Mansikkamäki, “An inkjet-deposited antenna for 2.4 GHz applications,” *International Journal of Electronics and Communications*, vol. 63, Jan. 2009, pp. 31-35.

[40] K. Lian, R. Li, H. Wang, J. Zhang, and D. Gamota, “Printed flexible memory devices using copper phthalocyanine,” *Materials Science and Engineering: B*, vol. 167, Feb. 2010, pp. 12-16.

[41] T. Sekitani, K. Zaitsu, Y. Noguchi, K. Ishibe, M. Takamiya, T. Sakurai, and T. Someya, “Printed Nonvolatile Memory for a Sheet-Type Communication System,” *IEEE Transactions on Electron Devices*, vol. 56, 2009, pp. 1027-1035.

[42] S. Sivaramakrishnan, P.-J. Chia, Y.-C. Yeo, L.-L. Chua, and P.K.-H. Ho, “Controlled insulator-to-metal transformation in printable polymer composites with nanometal clusters,” *Nature materials*, vol. 6, Feb. 2007, pp. 149-155.

[43] K. Crowley, A. Morrin, R.L. Shepherd, M. in het Panhuis, G.G. Wallace, M.R. Smyth, and A.J. Killard, “Fabrication of Polyaniline-Based Gas Sensors Using Piezoelectric Inkjet and Screen Printing for the Detection of Hydrogen Sulfide,” *IEEE Sensors Journal*, vol. 10, Sep. 2010, pp. 1419-1426.

[44] J. Jang, J. Ha, and J. Cho, “Fabrication of Water-Dispersible Polyaniline-Poly(4-styrenesulfonate) Nanoparticles For Inkjet-Printed Chemical-Sensor Applications,” *Advanced Materials*, vol. 19, Jul. 2007, pp. 1772-1775.

[45] T. Unander, H.-E. Nilsson, and B. Oelmann, “Printed touch sensor for interactive packaging and display,” *Proceedings of the 6th International Conference on Polymers and Adhesives in Microelectronics and Photonics*, Tokyo, Japan: 2007, pp. 12-17.

[46] T. Unander and H.-E. Nilsson, “Characterization of Printed Moisture Sensors in Packaging Surveillance Applications,” *IEEE Sensors Journal*, vol. 9, Aug. 2009, pp. 922-928.

[47] H.-E. Nilsson, H. Andersson, A. Manuilskiy, T. Unander, K. Hammarling, J. Sidén, and M. Gulliksson, “Printed Write Once and Read Many Sensor Memories in Smart Packaging Applications,” *IEEE Sensors Journal*, 2010, p. 7, DOI: 10.1109/JSEN.2010.2095496.

[48] K.E. Lilja, T.G. Bäcklund, D. Lupo, T. Hassinen, and T. Joutsenoja, “Gravure printed organic rectifying diodes operating at high frequencies,” *Organic Electronics*, vol. 10, Aug. 2009, pp. 1011-1014.

[49] J. Vaillancourt, H. Zhang, P. Vasinajindakaw, H. Xia, X. Lu, X. Han, D.C. Janzen, W.-S. Shih, C.S. Jones, M. Stroder, M.Y. Chen, H. Subbaraman, R.T. Chen, U. Berger, and M. Renn, “All ink-jet-printed carbon nanotube thin-film transistor on a polyimide substrate with an ultrahigh operating frequency of over 5 GHz,” *Applied Physics Letters*, vol. 93, 2008, p. 243301.

[50] M. Jung, J. Kim, J. Noh, N. Lim, C. Lim, G. Lee, J. Kim, H. Kang, K. Jung, A.D. Leonard, J.M. Tour, and G. Cho, “All-Printed and Roll-to-Roll-Printable 13.56-MHz-Operated 1-bit RF Tag on Plastic Foils,” *IEEE Transactions on Electron Devices*, vol. 57, 2010, pp. 571-580.

[51] K. Murata, J. Matsumoto, A. Tezuka, Y. Matsuba, and H. Yokoyama, “Super-fine ink-jet printing: toward the minimal manufacturing system,” *Microsystem Technologies*, vol. 12, Oct. 2005, pp. 2-7.

[52] T.-M. Lee, S.-H. Lee, J.-H. Noh, D.-S. Kim, and S. Chun, “The effect of shear force on ink transfer in gravure offset printing,” *Journal of Micromechanics and Microengineering*, vol. 20, Dec. 2010, p. 125026.

[53] J.R. Sheats, D. Biesty, J. Noel, and G.N. Taylor, “Printing technology for ubiquitous electronics,” *Circuit World*, vol. 36, 2010, pp. 40-47.

[54] J.R. Sheats, “Manufacturing and commercialization issues in organic electronics,” *Journal of Materials Research*, vol. 19, 2004, pp. 1974-1989.

[55] T.H.J. van Osch, J. Perelaer, A.W.M. de Laat, and U.S. Schubert, “Inkjet Printing of Narrow Conductive Tracks on Untreated Polymeric Substrates,” *Advanced Materials*, vol. 20, Jan. 2008, pp. 343-345.

[56] H.-H. Lee, K.-S. Chou, and K.-C. Huang, “Inkjet printing of nanosized silver colloids,” *Nanotechnology*, vol. 16, Oct. 2005, pp. 2436-2441.

[57] N.R. Bieri, J. Chung, S.E. Haferl, D. Poulikakos, and C.P. Grigoropoulos, “Microstructuring by printing and laser curing of nanoparticle solutions,” *Applied Physics Letters*, vol. 82, 2003, pp. 3529-3531.

[58] J. Chung, S. Ko, N.R. Bieri, C.P. Grigoropoulos, and D. Poulikakos, “Conductor microstructures by laser curing of printed gold nanoparticle ink,” *Applied Physics Letters*, vol. 84, 2004, pp. 801-803.

[59] S.H. Ko, H. Pan, C.P. Grigoropoulos, C.K. Luscombe, J.M.J. Fréchet, and D. Poulikakos, “All-inkjet-printed flexible electronics fabrication on a polymer substrate by low-temperature high-resolution selective laser sintering of metal nanoparticles,” *Nanotechnology*, vol. 18, Aug. 2007, p. 345202.

[60] T. Kumpulainen, J. Pekkanen, J. Valkama, J. Laakso, R. Tuokko, and M. Mäntysalo, “Low temperature nanoparticle sintering with continuous wave and pulse lasers,” *Optics & Laser Technology*, vol. 43, Apr. 2011, pp. 570-576.

[61] P. Laakso, S. Ruotsalainen, E. Halonen, M. Mäntysalo, and A. Kemppainen, “Sintering of printed nanoparticle structures using laser treatment,” *Proceedings of ICALEO 2009 - 28th International Congress on Applications of Lasers and Electro-Optics*, Orlando, US: 2009, pp. 1360-1366.

[62] H.-S. Kim, S.R. Dhage, D.-E. Shim, and H.T. Hahn, “Intense pulsed light sintering of copper nanoink for printed electronics,” *Applied Physics A*, vol. 97, Aug. 2009, pp. 791-798.

[63] T. Öhlund, J. Örtegren, H. Andersson, and H.-E. Nilsson, “Sintering Methods for Metal Nanoparticle Inks on Flexible Substrates,” *Proceedings of the 25th International Conference on Digital Printing Technologies*, Louisville, KY, US: 2009, pp. 614-617.

[64] J. West, M. Carter, S. Smith, and J. Sears, “Photonic Curing of Silver Nanoparticle Based Inks,” *Proceedings of NSTI-Nanotech 2010*, Anahaim, CA, USA: 2010, pp. 210-213.

[65] K.C. Yung, X. Gu, C.P. Lee, and H.S. Choy, “Ink-jet printing and camera flash sintering of silver tracks on different substrates,” *Journal of Materials Processing Technology*, vol. 210, Nov. 2010, pp. 2268-2272.

[66] J. Perelaer, B.-J. de Gans, and U.S. Schubert, “Ink-jet Printing and Microwave Sintering of Conductive Silver Tracks,” *Advanced Materials*, vol. 18, Aug. 2006, pp. 2101-2104.

[67] J. Perelaer, M. Klokkenburg, C.E. Hendriks, and U.S. Schubert, “Microwave Flash Sintering of Inkjet-Printed Silver Tracks on Polymer Substrates,” *Advanced Materials*, vol. 21, Dec. 2009, pp. 4830-4834.

[68] S. Magdassi, M. Grouchko, O. Berezin, and A. Kamyshny, “Triggering the sintering of silver nanoparticles at room temperature,” *ACS nano*, vol. 4, Apr. 2010, pp. 1943-1948.

[69] W. Zapka, W. Voil, C. Loderer, and P. Lang, “Low Temperature Chemical Post-Treatment of Inkjet Printed Nano-Particle Silver Inks,” *Proceedings of NIP24 and Digital Fabrication*, 2008, pp. 906-911.

[70] D. Wakuda, C.-J. Kim, K.-S. Kim, and K. Suganuma, “Room temperature sintering mechanism of Ag nanoparticle paste,” *Proceedings of the 2nd Electronics Systemintegration Technology Conference*, Greenwich, UK: 2008, pp. 909-914.

[71] I. Reinhold, C.E. Hendriks, R. Eckardt, J.M. Kranenburg, J. Perelaer, R.R. Baumann, and U.S. Schubert, “Argon plasma sintering of inkjet printed silver tracks on polymer substrates,” *Journal of Materials Chemistry*, vol. 19, 2009, pp. 3384-3388.

[72] S.R. Forrest, “The path to ubiquitous and low-cost organic electronic appliances on plastic,” *Nature*, vol. 428, 2004, pp. 911-918.

[73] A.C. Huebler, F. Doetz, H. Kempa, H.E. Katz, M. Bartzsch, N. Brandt, I. Hennig, U. Fuegmann, S. Vaidyanathan, J. Granstrom, S. Liu, A. Sydorenko, T. Zillger, G. Schmidt, K. Preissler, E. Reichmanis, P. Eckerle, F. Richter, T. Fischer, and U. Hahn, “Ring oscillator fabricated completely by means of mass-printing technologies,” *Organic Electronics*, vol. 8, Oct. 2007, pp. 480-486.

[74] C. Lee, H. Kang, C. Kim, and K. Shin, “A Novel Method to Guarantee the Specified Thickness and Surface Roughness of the Roll-to-Roll Printed Patterns Using the Tension of a Moving Substrate,” *Journal of Microelectromechanical Systems*, vol. 19, 2010, pp. 1243-1253.

[75] J. Noh, D. Yeom, C. Lim, H. Cha, J. Han, J. Kim, Y. Park, and V. Subramanian, “Scalability of Roll-to-Roll Gravure-Printed Electrodes on Plastic Foils,” *IEEE Transactions on Electronics Packaging Manufacturing*, vol. 33, 2010, pp. 275-283.

[76] T. Mäkelä, S. Jussila, H. Kosonen, T.G. Bäcklund, H.G.O. Sandberg, and H. Stubb, "Utilizing roll-to-roll techniques for manufacturing source-drain electrodes for all-polymer transistors," *Synthetic Metals*, vol. 153, Sep. 2005, pp. 285-288.

[77] M. Luniak, H.-P. Monser, V. Brod, and K.-J. Wolter, "Smart label uses polymer thick film technology on low-cost substrates," *Proceedings of the First International IEEE Conference on Polymers and Adhesives in Microelectronics and Photonics*, Potsdam, Germany: 2001, pp. 314-318.

[78] F.C. Krebs, M. Jørgensen, K. Norrman, O. Hagemann, J. Alstrup, T.D. Nielsen, J. Fyenbo, K. Larsen, and J. Kristensen, "A complete process for production of flexible large area polymer solar cells entirely using screen printing—First public demonstration," *Solar Energy Materials and Solar Cells*, vol. 93, Apr. 2009, pp. 422-441.

[79] J.R. Dorfman, D.K. Anderson, and V. Arancio, "Advanced Screen Printable Thin Film PV Front Side Silver Conductor Compositions," *Proceedings of the 34th IEEE Photovoltaic Specialists Conference (PVSC)*, 2009, pp. 2477-2479.

[80] Z. Bao, Y. Feng, A. Dodabalapur, V.R. Raju, and A.J. Lovinger, "High-Performance Plastic Transistors Fabricated by Printing Techniques," *Chemistry of Materials*, vol. 9, 1997, pp. 1299-1301.

[81] M. Singh, H.M. Haverinen, P. Dhagat, and G.E. Jabbour, "Inkjet Printing - Process and Its Applications," *Advanced materials*, vol. 22, Feb. 2010, pp. 673-685.

[82] E. Tekin, P.J. Smith, and U.S. Schubert, "Inkjet printing as a deposition and patterning tool for polymers and inorganic particles," *Soft Matter*, vol. 4, 2008, pp. 703-713.

[83] B.Y. Ahn, E.B. Duoss, M.J. Motala, X. Guo, S.-I. Park, Y. Xiong, J. Yoon, R.G. Nuzzo, J.A. Rogers, and J.A. Lewis, "Omnidirec-

tional printing of flexible, stretchable, and spanning silver microelectrodes," *Science*, vol. 323, Mar. 2009, pp. 1590-1593.

[84] B.E. Kahn, "The M3D aerosol jet system, an alternative to inkjet printing for printed electronics," *Organic and Printed Electronics*, vol. 1, 2007, pp. 14-17.

[85] K.W. Whites, T. Amert, S.M. Woessner, N.-S. Kim, S. Decker, and J. Kellar, "Direct-Write Printing of Multilayered Appliqué Antennas on High Impedance Surfaces," *Proceedings of the IEEE Antennas and Propagation Society International Symposium (APSURSI)*, Honolulu, HI, USA: 2007, pp. 2765-2768.

[86] V. Pekkanen, K. Kaija, M. Mäntysalo, E. Kunnari, J. Niittynen, and P. Mansikkamäki, "Functional fluid jetting performance optimization," *Microelectronics Reliability*, vol. 50, Jun. 2010, pp. 864-871.

[87] I.M. Hutchings, "Ink-jet printing in micro-manufacturing: opportunities and limitations," *Proceedings of 4M/ICOMM 2009 - The Global Conference on Micro Manufacture*, Karlsruhe, Germany: 2009, pp. 47-57.

[88] B. Derby, "Inkjet Printing of Functional and Structural Materials: Fluid Property Requirements, Feature Stability, and Resolution," *Annual Review of Materials Research*, vol. 40, Jun. 2010, pp. 395-414.

[89] V. Subramanian, P.C. Chang, J.B. Lee, S.E. Molesa, and S.K. Volkman, "Printed organic transistors for ultra-low-cost RFID applications," *IEEE Transactions on Components and Packaging Technologies*, vol. 28, Dec. 2005, pp. 742-747.

[90] M. Mengel and I. Nikitin, "Inkjet printed dielectrics for electronic packaging of chip embedding modules," *Microelectronic Engineering*, vol. 87, Apr. 2010, pp. 593-596.

[91] J. Stringer and B. Derby, “Formation and stability of lines produced by inkjet printing,” *Langmuir*, vol. 26, Jun. 2010, pp. 10365-10372.

[92] M. Mäntysalo, V. Pekkanen, K. Kaija, J. Niittynen, S. Koskinen, E. Halonen, P. Mansikkamäki, and O. Hämeenoja, “Capability of inkjet technology in electronics manufacturing,” *Proceedings of the 59th Electronic Components and Technology Conference*, San Diego, CA, USA: 2009, pp. 1330-1336.

[93] A. Gregg, L. York, and M. Strnad, “Roll-to-Roll Manufacturing of Flexible Displays,” *Flexible Flat Panel Displays*, John Wiley & Sons, Ltd, 2005, pp. 409-445.

[94] J. Puetz and M.A. Aegerter, “Direct gravure printing of indium tin oxide nanoparticle patterns on polymer foils,” *Thin Solid Films*, vol. 516, May. 2008, pp. 4495-4501.

[95] S. Jang, Y. Seo, J. Choi, T. Kim, J. Cho, S. Kim, and D. Kim, “Sintering of inkjet printed copper nanoparticles for flexible electronics,” *Scripta Materialia*, vol. 62, Mar. 2010, pp. 258-261.

[96] B. Lee, Y. Kim, S. Yang, I. Jeong, and J. Moon, “A low-cure-temperature copper nano ink for highly conductive printed electrodes,” *Current Applied Physics*, vol. 9, Mar. 2009, p. e157-e160.

[97] B.K. Park, D. Kim, S. Jeong, J. Moon, and J.S. Kim, “Direct writing of copper conductive patterns by ink-jet printing,” *Thin Solid Films*, vol. 515, Jul. 2007, pp. 7706-7711.

[98] M.-C. Daniel and D. Astruc, “Gold nanoparticles: assembly, supramolecular chemistry, quantum-size-related properties, and applications toward biology, catalysis, and nanotechnology,” *Chemical reviews*, vol. 104, Jan. 2004, pp. 293-346.

[99] I. Pastoriza-Santos and L.M. Liz-Marzán, "Formation of PVP-Protected Metal Nanoparticles in DMF," *Langmuir*, vol. 18, Apr. 2002, pp. 2888-2894.

[100] W.P. Halperin, "Quantum size effects in metal particles," *Reviews of Modern Physics*, vol. 58, 1986, pp. 533-607.

[101] P. Buffat and J.-P. Borel, "Size effect on the melting temperature of golf particles*," *Physical Review A*, vol. 13, 1976, pp. 2287-2298.

[102] T. Castro, R. Reifenberger, E. Choi, and R.P. Andres, "Size-dependent melting temperature of individual nanometer-sized metallic clusters," *Physical Review B*, vol. 42, 1990, pp. 8548-8557.

[103] W. Luo, W. Hu, and S. Xiao, "Size Effect on the Thermodynamic Properties of Silver Nanoparticles," *Journal of Physical Chemistry C*, vol. 112, Feb. 2008, pp. 2359-2369.

[104] M. Wautelet, "Estimation of the variation of the melting temperature with the size of small particles, on the basis of a surface-phonon instability model," *Journal of Physics D: Applied Physics*, vol. 24, 1990, pp. 343-346.

[105] Q. Jiang, S. Zhang, and M. Zhao, "Size-dependent melting point of noble metals," *Materials Chemistry and Physics*, vol. 82, Sep. 2003, pp. 225-227.

[106] K.K. Nanda, S.N. Sahu, and S.N. Behera, "Liquid-drop model for the size-dependent melting of low-dimensional systems," *Physical Review A*, vol. 66, Jul. 2002, p. 013208.

[107] M. Schmidt, R. Kusche, B. von Issendorff, and H. Haberland, "Irregular variations in the melting point of size-selected atomic clusters," *Nature*, vol. 393, 1998, pp. 238-240.

[108] B. Gilbert, F. Huang, H. Zhang, G.A. Waychunas, and J.F. Banfield, “Nanoparticles: strained and stiff.,” *Science*, vol. 305, Jul. 2004, pp. 651-654.

[109] Y. Lee, J.-rak Choi, K.J. Lee, N.E. Stott, and D. Kim, “Large-scale synthesis of copper nanoparticles by chemically controlled reduction for applications of inkjet-printed electronics,” *Nanotechnology*, vol. 19, Oct. 2008, p. 415604.

[110] M. José-Yacaman, C. Gutierrez-Wing, M. Miki, D.-Q. Yang, K.N. Piyakis, and E. Sacher, “Surface diffusion and coalescence of mobile metal nanoparticles,” *Journal of physical chemistry B*, vol. 109, May. 2005, pp. 9703-9711.

[111] J. Perelaer, A.W.M. de Laat, C.E. Hendriks, and U.S. Schubert, “Inkjet-printed silver tracks: low temperature curing and thermal stability investigation,” *Journal of Materials Chemistry*, vol. 18, 2008, pp. 3209-3215.

[112] D.L. Johnson, “New Method of Obtaining Volume, Grain-Boundary, and Surface Diffusion Coefficients from Sintering Data,” *Journal of Applied Physics*, vol. 40, 1969, pp. 192-200.

[113] S.H. Ko, H. Pan, D.J. Hwang, J. Chung, S. Ryu, C.P. Grigoropoulos, and D. Poulikakos, “High resolution selective multilayer laser processing by nanosecond laser ablation of metal nanoparticle films,” *Journal of Applied Physics*, vol. 102, 2007, p. 093102.

[114] M. Grouchko, A. Kamyshny, C.F. Mihailescu, D.F. Anghel, and S. Magdassi, “Conductive inks with a ‘built-in’ mechanism that enables sintering at room temperature,” *ACS nano*, vol. 5, Apr. 2011, pp. 3354-3359.

[115] P.B. Sarawade, J.-K. Kim, A. Hilonga, and H.T. Kim, “Preparation of hydrophobic mesoporous silica powder with a high specific surface area by surface modification of a wet-gel slurry and spray-drying,” *Powder Technology*, vol. 197, Jan. 2010, pp. 288-294.

[116] S. Lu, E.M. Pearce, and T.K. Kwei, “Blends and Interpolymer Complexes of Poly(Styrene-Co-4-Vinylphenylmethylphenylsilanol) and Poly(N-Vinylpyrrolidone),” vol. 7, 1996, pp. 553-559.

[117] Y.-K. Han, E.M. Pearce, and T.K. Kwei, “Poly(styrene- b -vinylphenyldimethylsilanol) and Its Blends with Homopolymers,” *Macromolecules*, vol. 33, Feb. 2000, pp. 1321-1329.

[118] E. Kunnari, J. Valkama, M. Keskinen, and P. Mansikkamäki, “Environmental evaluation of new technology: printed electronics case study,” *Journal of Cleaner Production*, vol. 17, Jun. 2009, pp. 791-799.

[119] V. Subramanian, J.B. Chang, A. de la Fuente Vornbrock, D.C. Huang, L. Jagannathan, F. Liao, B. Mattis, S. Molesa, D.R. Redinger, D. Soltman, S.K. Volkman, and Q. Zhang, “Printed Electronics for Low-Cost Electronic Systems: Technology Status and Application Development,” *Proceedings of the 38th European Solid-State Device Research Conference (ESSDERC)*, Edinburgh, UK: 2008, pp. 17-24.

[120] S. Magdassi, A. Bassa, Y. Vinetsky, and A. Kamyshny, “Silver Nanoparticles as Pigments for Water-Based Ink-Jet Inks,” *Chemistry of Materials*, vol. 15, Jun. 2003, pp. 2208-2217.

[121] J.B. Szczech, C.M. Megaridis, D.R. Gamota, and J. Zhang, “Fine-line conductor manufacturing using drop-on demand PZT printing technology,” *IEEE Transactions on Electronics Packaging Manufacturing*, vol. 25, Jan. 2002, pp. 26-33.

[122] J. Perelaer, C.E. Hendriks, A.W.M. de Laat, and U.S. Schubert, “One-step inkjet printing of conductive silver tracks on polymer substrates,” *Nanotechnology*, vol. 20, Apr. 2009, p. 165303.

[123] P.J. Smith, D.-Y. Shin, J.E. Stringer, B. Derby, and N. Reis, “Direct ink-jet printing and low temperature conversion of conductive

silver patterns," *Journal of Materials Science*, vol. 41, May. 2006, pp. 4153-4158.

[124] C.D. Muller, A. Falcou, N. Reckefuss, M. Rojahn, V. Wiederhirn, P. Rudati, H. Frohne, O. Nuyken, H. Becker, and K. Meerholz, "Multi-colour organic light-emitting displays by solution processing," *Nature*, vol. 421, 2003, pp. 829-833.

[125] L. Zhou, A. Wanga, S.-C. Wu, J. Sun, S. Park, and T.N. Jackson, "All-organic active matrix flexible display," *Applied Physics Letters*, vol. 88, 2006, p. 083502.

[126] K. Neyts, A. Real, M. Marescaux, S. Mladenovski, and J. Beeckman, "Conductor grid optimization for luminance loss reduction in organic light emitting diodes," *Journal of Applied Physics*, vol. 103, 2008, p. 093113.

[127] S. Choi, W.J. Potscavage, and B. Kippelen, "Area-scaling of organic solar cells," *Journal of Applied Physics*, vol. 106, 2009, p. 054507.

[128] C. May, Y. Tomita, M. Toerker, M. Eritt, F. Loeffler, J. Amelung, and K. Leo, "In-line deposition of organic light-emitting devices for large area applications," *Thin Solid Films*, vol. 516, May. 2008, pp. 4609-4612.

[129] T. Aernouts, P. Vanlaeke, W. Geens, J. Poortmans, P. Heremans, S. Borghs, R. Mertens, R. Andriessen, and L. Leenders, "Printable anodes for flexible organic solar cell modules," *Thin Solid Films*, vol. 451-452, Mar. 2004, pp. 22-25.

[130] K. Tvingstedt and O. Inganäs, "Electrode Grids for ITO-free Organic Photovoltaic Devices," *Advanced Materials*, vol. 19, Oct. 2007, pp. 2893-2897.

[131] F.C. Krebs, “All solution roll-to-roll processed polymer solar cells free from indium-tin-oxide and vacuum coating steps,” *Organic Electronics*, vol. 10, Aug. 2009, pp. 761-768.

[132] M. Glatthaar, M. Niggemann, B. Zimmermann, P. Lewer, M. Riede, A. Hinsch, and J. Luther, “Organic solar cells using inverted layer sequence,” *Thin Solid Films*, vol. 491, Nov. 2005, pp. 298-300.

[133] M. Grätzel, “Solar energy conversion by dye-sensitized photovoltaic cells,” *Inorganic chemistry*, vol. 44, Oct. 2005, pp. 6841-6851.

[134] S. Sarma, *Towards the five-cent tag*, Auto ID White Paper MIT-AUTOID-WH-006: 2001.

[135] Y. Yasuda, E. Ide, and T. Morita, “Low-Temperature Bonding Using Silver Nanoparticles Stabilized by Short-Chain Alkylamines,” *Japanese Journal of Applied Physics*, vol. 48, Dec. 2009, p. 125004.

[136] J.G. Bai and G.-Q. Lu, “Thermomechanical Reliability of Low-Temperature Sintered Silver Die Attached SiC Power Device Assembly,” *IEEE Transactions on Device and Materials Reliability*, vol. 6, Sep. 2006, pp. 436-441.

[137] J.-W. Kim, Y.-C. Lee, J.-M. Kim, W. Nah, H.-S. Lee, H.-C. Kwon, and S.-B. Jung, “Characterization of direct patterned Ag circuits for RF application,” *Microelectronic Engineering*, vol. 87, Mar. 2010, pp. 379-382.

[138] B. Shao, R. Weerasekera, L.-R. Zheng, R. Liu, W. Zapka, and P. Lindberg, “High Frequency Characterization of Inkjet Printed Coplanar Waveguides,” *Proceedings of the12th IEEE Workshop on Signal Propagation on Interconnects (SPI)*, Avignon, France: 2008, pp. 1-4.

[139] H.-J. Lee, S. Seo, K. Yun, J.W. Joung, I.-Y. Oh, and J.-G. Yook, "RF performance of CPW transmission line fabricated with inkjet printing technology," *Proceedings of Asia-Pacific Microwave Conference (APMC)*, 2008, pp. 1-4.

[140] V.J. Pynttäri, R.M. Mäkinen, V.K. Palukuru, K. Östman, H.P. Sillanpää, T. Kanerva, T. Lepistö, J. Hagberg, and H. Jantunen, "Application of Wide-Band Material Characterization Methods to Printable Electronics," *IEEE Transactions on Electronics Packaging Manufacturing*, vol. 33, Jul. 2010, pp. 221-227.

[141] A. Chiolerio, G. Maccioni, P. Martino, M. Cotto, P. Pandolfi, P. Rivolo, S. Ferrero, and L. Scaltrito, "Inkjet printing and low power laser annealing of silver nanoparticle traces for the realization of low resistivity lines for flexible electronics," *Microelectronic Engineering*, Jan. 2011, p. 3, DOI: 10.1016/j.mee.2010.12.099.

[142] A.K. Sowpati, V.K. Palukuru, V. Pynttäri, R. Mäkinen, M.V. Kartikeyan, and H. Jantunen, "Performance of printable antennas with different conductor thickness," *Progress in Electromagnetics Research Letters*, vol. 13, 2010, pp. 59-65.

[143] K. Kirschenmann, K.W. Whites, and S.M. Woessner, "Inkjet printed microwave frequency multilayer antennas," *Proceedings of the IEEE Antennas and Propagation International Symposium (APSURSI)*, Honolulu, HI, USA: 2007, pp. 924-927.

[144] K. Finkenzeller, *RFID Handbook*, 2nd ed., John Wiley & Sons, Ltd., 2003.

[145] Z.N. Chen, *Antennas for portable devices*, John Wiley & Sons, Ltd., 2007.

[146] The Palomar Project, *"Passive long distance multiple access UHF RFID system,"* Public report, European Commission, Project number IST1999-10339: 2002.

[147] J.D. Kraus, *Antennas*, New York: McGraw-Hill, 1950.

[148] P. Pursula, M. Hirvonen, K. Jaakkola, and T. Varpula, "Antenna Effective Aperture Measurement With Backscattering Modulation," *IEEE Transactions on Antennas and Propagation*, vol. 55, Oct. 2007, pp. 2836-2843.

[149] J. Siden, T. Olsson, A. Koptioug, and H.-E. Nilsson, "Reduced Amount of Conductive Ink with Gridded Printed Antennas," *Proceedings of the 5th International Conference on Polymers and Adhesives in Microelectronics and Photonics (Polytronic)*, Wroclaw, Poland: 2005, pp. 86-89.

[150] N. Lim, J. Kim, S. Lee, N. Kim, and G. Cho, "Screen Printed Resonant Tags for Electronic Article Surveillance Tags," *IEEE Transactions on Advanced Packaging*, vol. 32, 2009, pp. 72-76.

[151] S. Möller, C. Perlov, W. Jackson, C. Taussig, and S.R. Forrest, "A polymer/semiconductor write-once read-many-times memory," *Nature*, vol. 426, Nov. 2003, pp. 166-169.

[152] J. Ouyang, C.-W. Chu, R.J.-H. Tseng, A. Prakash, and Y. Yang, "Organic Memory Device Fabricated Through Solution Processing," *Proceedings of the IEEE*, vol. 93, 2005, pp. 1287-1296.

[153] N. Gergel-Hackett, B. Hamadani, B. Dunlap, J. Suehle, C. Richter, C. Hacker, and D. Gundlach, "A Flexible Solution-Processed Memristor," *IEEE Electron Device Letters*, vol. 30, Jul. 2009, pp. 706-708.

[154] S.-J. Kim and J.-S. Lee, "Flexible organic transistor memory devices," *Nano letters*, vol. 10, Aug. 2010, pp. 2884-2890.

[155] N. Johansson, "Volume manufacturing of printed non-volatile memories," *presented at Printed Electronics Asia*, Tokyo, Japan: 2009.

[156] H. Andersson, A. Rusu, A. Manuilskiy, S. Haller, S. Ayöz, and H.-E. Nilsson, "System of nano-silver inkjet printed memory cards and PC card reader and programmer," *Microelectronics Journal*, vol. 42, Jan. 2011, pp. 21-27.

[157] C. Werner, G. Behrens, K.-H. Hellbernd, D. Godlinski, V. Zöllmer, and M. Busse, "Electrical sintering of printed metal structures for mechanical sensors," *Proceedings of LOPE-C*, Frankfurt, Germany: 2011, pp. 192-195.

[158] Z.Z. Fang and H. Wang, "Densification and grain growth during sintering of nanosized particles," *International Materials Reviews*, vol. 53, Nov. 2008, pp. 326-352.

Errata

In publication [V], in section II, equation (1)

$$A_{eff} = \eta \frac{\lambda^2 G_r}{4\pi} \frac{4R_r R_T}{\left(R_r + R_T\right)^2 + \left(X_A + X_T\right)^2}$$

contains a misprint and should stand

$$A_{eff} = \eta \frac{\lambda^2 D_r}{4\pi} \frac{4R_r R_T}{\left(R_r + R_T\right)^2 + \left(X_A + X_T\right)^2},$$

where η is the radiation efficiency, λ is the wavelength in free space, D_r is the directivity of the tag antenna, R_r the antenna feed resistance, X_A the antenna feed reactance, R_T the load resistance, and X_T the load reactance. This misprint (antenna gain $G_\mathrm{r} = \eta D_\mathrm{r}$ in place of directivity) does not affect the results, analysis or the conclusions of publication [V].

Aalto-DD 81/2011

Electronic components and devices can be fabricated by printing engineered materials onto a substrate. In this work, for example, electric conductors, antennas and memory cards are printed using silver nanoparticle inks. Nanoparticles have unique characteristics that allow them to partially melt and sinter at low temperatures to form a continuous percolating structure. The electrical sintering method, introduced and developed in this Thesis, is implemented by coupling an electric field across the nanoparticle structure. The method can outperform conventional oven sintering in terms of speed, sintering efficiency and energy usage, and facilitates real-time monitoring and process control. Also another approach, where sintering is triggered through interaction between the ink and the coating layer of the printing substrate, is presented. The method enables direct component attachment to printed conductors. The methods and applications developed in this Thesis may become widely exploited in future printed electronics systems and manufacturing processes.

ISBN 978-952-60-4278-7 (pdf)
ISBN 978-952-60-4277-0
ISSN-L 1799-4934
ISSN 1799-4942 (pdf)
ISSN 1799-4934

Aalto University
School of Electrical Engineering
Department of Radio Science and Engineering
www.aalto.fi

BUSINESS + ECONOMY

ART + DESIGN + ARCHITECTURE

SCIENCE + TECHNOLOGY

CROSSOVER

DOCTORAL DISSERTATIONS